Department of Applied Physics, Low Temperature Laboratory

Nonlinearities and quantum phenomena in nanoelectromechanical systems

Raphaël Khan

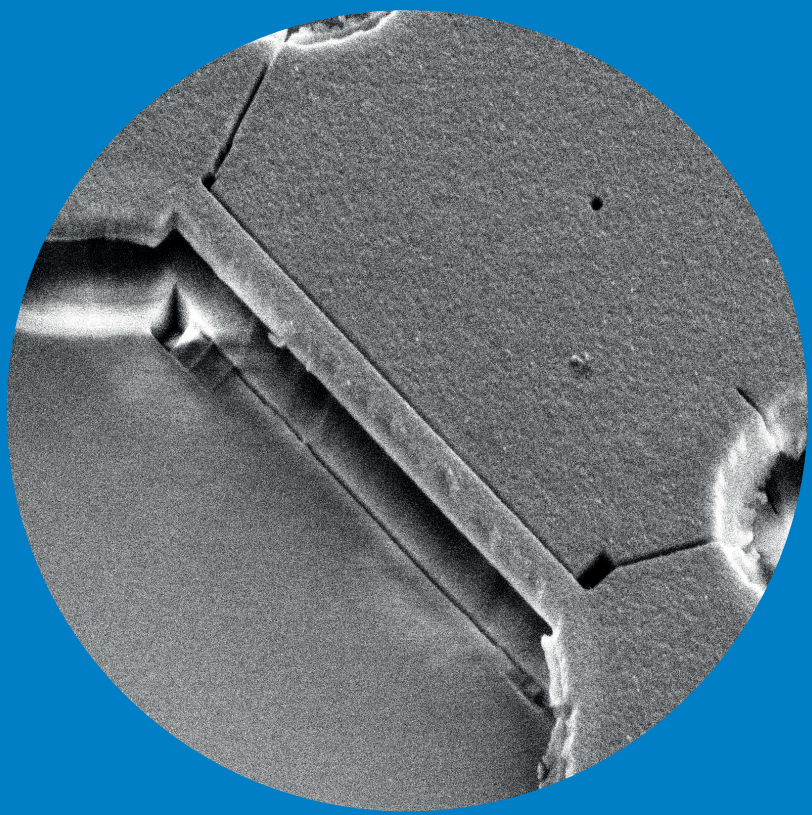

Aalto University

DOCTORAL DISSERTATIONS

Aalto University publication series
DOCTORAL DISSERTATIONS 145/2015

Nonlinearities and quantum phenomena in nanoelectromechanical systems

Raphaël Khan

A doctoral dissertation completed for the degree of Doctor of Science (Technology) to be defended, with the permission of the Aalto University School of Science, at a public examination held at the lecture hall M232 of the main building, Otakaari 1, on 16 October 2015 at 12:00.

Aalto University
School of Science
Department of Applied Physics, Low Temperature Laboratory

Supervising professor
Prof. Pertti Hakonen

Thesis advisor
Prof. Tero Heikkilä

Preliminary examiners
Prof. David Vitali, University of Camerino, Italy
Assoc. Prof. Andreas Isacsson, Chalmers University of Technology, Sweden

Opponent
Prof. Mats Jonson, Chalmers University of Technology, Sweden

Aalto University publication series
DOCTORAL DISSERTATIONS 145/2015

ISBN 978-952-60-6401-7 (printed)
ISBN 978-952-60-6402-4 (pdf)
ISSN-L 1799-4934
ISSN 1799-4934 (printed)
ISSN 1799-4942 (pdf)
http://urn.fi/URN:ISBN:978-952-60-6402-4

Unigrafia Oy
Helsinki 2015

Finland

441 697
Printed matter

Aalto University

Abstract

Aalto University, P.O. Box 11000, FI-00076 Aalto www.aalto.fi

Author
Raphaël Khan

Name of the doctoral dissertation
Nonlinearities and quantum phenomena in nanoelectromechanical system

Publisher School of Science

Unit Department of Applied Physics

Series Aalto University publication series DOCTORAL DISSERTATIONS 145/2015

Field of research Theoretical Physics

Manuscript submitted 11 May 2015 **Date of the defence** 16 October 2015

Permission to publish granted (date) 15 September 2015 **Language** English

☐ **Monograph** ☒ **Article dissertation (summary + original articles)**

Abstract

This dissertation addresses different types of nonlinear phenomena in nanoelectromechanical systems (NEMS) with an aim to find quantum behavior in them. Quantum mechanics is a theory that describes physics at the atomic scale. Without it many phenomena such as the electronic properties of crystalline matter would not be properly understood. However, the way the world works on quantum scale is nothing like how it appears in the classical perception of human beings. Although all the objects around us are made of atoms, none of the objects show quantum behavior since perturbations coming from their surroundings destroy the quantum states. During the last decade, NEMS have caught the interest of the scientific community since they are promising candidates to study and test quantum mechanics in the macroscopic scale.

In recent experiments, optomechanical systems have been used to cool nanomechanical resonators to their ground state. Ground state cooling is a requirement for the observation of the quantum nature of the mechanical resonator. But in addition to being close to the ground state, nonlinearities are needed to distinguish the quantum behavior from the classical one. Therefore, great effort is spent studying nonlinearities either within the mechanical resonator or due to an external system coupled to the nanomechanical resonator.

This dissertation is composed of an introduction and four research articles published in high-level physics journals. The introduction starts by discussing the basic theory of NEMS. Then it specifies some relevant nonlinearities that occur in nanoelectromechanical systems, and how one can use them for the observation of quantum phenomena on macroscopic scale. The details of such nonlinearities are described in the research articles presented in the thesis.

Keywords NEMS, Nonlinearities, Quantum Mechanics

ISBN (printed) 978-952-60-6401-7 **ISBN (pdf)** 978-952-60-6402-4

ISSN-L 1799-4934 **ISSN (printed)** 1799-4934 **ISSN (pdf)** 1799-4942

Location of publisher Helsinki **Location of printing** Helsinki **Year** 2015

Pages 96 **urn** http://urn.fi/URN:ISBN:978-952-60-6402-4

Preface

The research presented in this thesis is the result of work conducted during the years 2010-2015 in the O. V. Lounasmaa Laboratory of Aalto University previously known as the Low Temperature Laboratory of the Helsinki University of Technology. In addition to being an interesting place for me to work it has also offered me the possibilty to discuss with the most enthusiastic and knowledgeable people I have ever met. I would like to acknowledge all here who have helped to make this journey possible.

First and foremost I wish to express my gratitude to my instructor and previous head of the theory group of O. V. Lounasmaa Laboratory, Prof. Tero Heikkilä, for his guidance during the completion of this dissertation. I have not been the easiest student but his patience, support and commitment have helped me to complete my thesis

I want to thank my supervisor and director of our lab, Prof. Pertti Hakonen for our discussions about experiments related to my research and for the tremendous amount of work he puts in to make the lab run and to be such a rewarding place to work.

I am especially grateful for the guidance of Dr. Francesco Massel who dedicated his time and guidance for helping me to finish this thesis. Without him this dissertation would not exist.

The atmosphere in the lab wouldn't be as nice without my friends and colleagues who have made my time in the lab enjoyable. I would especially like to thank Ville Kauppila, Daniel Cox, Antti Puska, Matthias Brandt, Karthikeyan Kumar, Juha Pirkkalainen, Matti Tomi and Sergeil Danilin. I would like also to thank my former colleagues and friends Matti Laakso and Juha Voutilainen for introducing me to the Finnish culture. To me you are my Finnish big brothers.

Doing research is hard and it is easy to become isolated. Fortunately

my friends were there to take my mind away from work. Thanks to Olivier Thomann, Stephane Derom, Emile Maras and Florence Linez for our lunches together which created a real break during my work days.

Finally I would like to thank my parents Ahsan and Danièle and my sister Elodie for always being there for me and encouraging me in pursuing my studies and Mia-Marisa for supporting me in the hardest moments during the completion of this dissertation.

Helsinki, September 6, 2015,

Raphael KHAN

Contents

List of Publications

This thesis consists of an overview and of the following publications which are referred to in the text by their Roman numerals.

I Mika A. Sillanpää, Raphaël Khan, Tero T. Heikkilä, and Pertti J. Hakonen. Macroscopic quantum tunneling in nanoelectromechanical systems. *Physical Review B*, 84, 195433, November 2011.

II Raphaël Khan, F. Massel, and T. T. Heikkilä. Tension-induced nonlinearities of flexural modes in nanomechanical resonators. *Physical Review B*, 87, 235406, June 2013.

III T. T. Heikkilä, F. Massel, J. Tuorila, R. Khan and M. A. Sillanpää. Enhancing Optomechanical Coupling via the Josephson Effect. *Physical Review Letters*, 112, 203603, May 2014.

IV R. Khan F. Massel, T. T. Heikkilä. Cross-Kerr nonlinearity in optomechanical systems. *Physical Review A*, 91, 043822, April 2015.

Author's Contribution

Publication I: "Macroscopic quantum tunneling in nanoelectromechanical systems"

The author made all the numerical computations and made the simulations for observing quantum tunneling for the graphene based resonator and carbon nanotube resonator.

Publication II: "Tension-induced nonlinearities of flexural modes in nanomechanical resonators"

The author obtained most of the analytical results and made all the numerical computations. The author also contributed to writing the paper.

Publication III: "Enhancing Optomechanical Coupling via the Josephson Effect"

The author helped in the derivation of the analytical results. Especially the author helped with the derivation of the Hamiltonian and with the Schrieffer-Wolff calculation.

Publication IV: "Cross-Kerr nonlinearity in optomechanical systems"

The author derived most of the analytical results and tried different approaches for solving the problem. The author made all of the numerical computations and was also in charge of writing the paper.

1. Introduction

Mechanical devices have long been used as sensors for measuring quantities such as mass, force, displacement and speed. These devices were used as early as the times of antiquity and they have been used to establish fundamental laws of physics. For example the Coulomb torsional balance [1] was used to determine the distance dependence of the interaction between electrically charged particles and Cavendish's experiment [2] to measure the force of gravity between masses and to give a value for the gravitational constant.

Today the most modern version of mechanical sensors are nanoelectromechanical systems (NEMS). They consist of a suspended nano-beam coupled to an electronic device which actuates (drives) and transduces (detects) its motion. Such a system can be a charged beam close to a gate (Fig. 1.1) in which case a time dependent electric force between the gate and the beam makes the latter vibrate. NEMS are used similarly to the mechanical systems mentioned above, that is to say as sensors such as force, charge or mass detectors [3, 4, 5, 6], but their sensitivity has been pushed so far that it is now possible to measure mass with a resolution of $10^{-24}\,\mathrm{g}$ which corresponds to the mass of one proton [6]. In addition NEMS also offer the possibility to measure quantum phenomena such as the Casimir force [7] which arises from the fluctuations of the electromagnetic field between two metallic plates.

In addition, continual progress in making ever smaller resonators has lead to the increase of the frequency ω at which their modes vibrate. The frequency of the vibration is typically between a few Megahertz and one Gigahertz. With these high frequencies it is possible to reach a temperature T where the thermal energy $k_b T$ becomes smaller than the quantum energy $\hbar\omega$ of the resonator. This makes it possible to cool the mode of vibration to its ground state. Pioneering work in cooling the mechanical

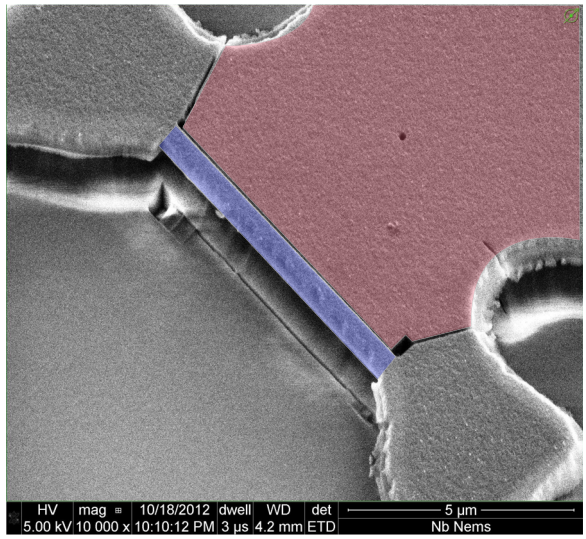

Figure 1.1. SEM (scanning electron microscope) picture of a nanoelectromechanical device. It consists of a niobium (Nb) beam (in blue) of length $7\,\mu\mathrm{m}$, width $480\,\mathrm{nm}$ and thickness $100\,\mathrm{nm}$. The gap between the gate (in red) and the beam is $26\,\mathrm{nm}$.Courtesy of Matthias Brandt, Aalto University.

resonator to its ground state was achieved in 2010 by Andrew Cleland's group [8]. In their work the ground state was reached by using cryogenic refrigeration to cool a high frequency (6 GHz) piezoelectric mode to its ground state.

A year later the ground state of a vibrational mode with frequency of the order of a few Megahertz was reached by coupling it to a microwave cavity [9]. This field is known as cavity optomechanics and has developed rapidly in the past few years. Cavity optomechanics offers a framework to study the interaction between an electromagnetic field and the vibrations of a mechanical resonator. The interation between the cavity and the resonator is mediated by the radiation-pressure force. It is this force which has been used in [9] to alter the vibrations of the mechanical resonator and to transfer energy from the resonator to the cavity leading to the cooling of the mechanical resonator.

The possibility to cool a mode of vibrations close to its ground state, has offered the opportunity of observing quantum phenomena within the mechanical system itself. Many proposals of quantum behavior such as superposition of states [10] or quantum squeezed states [11, 12, 13, 14] have been suggested. However, to observe quantum phenomena in NEMS, it is crucial to go beyond linear regime where it is not possible to distinguish classical behavior from the quantum one. Indeed as the correspondence

principle states, for a linear system the classical equation of motion is the same as the quantum one. Therefore, in order to observe quantum behavior nonlinearity is needed.

This thesis is an article dissertation in which I discuss various nonlinear effects that occur in NEMS. The aim of this thesis is to give the reader the basic tools and concepts used in the published articles as well as a brief overview of their outcomes. This thesis is divided into three parts. In the first chapter I introduce the basic theory for describing the deformation of a resonator. In the second chapter I discuss the nonlinear effects arising in NEMS due to large deformations. Both Chapter 1 and 2 are the basis of the articles in this dissertation, especially for Publication I and Publication II. Finally I introduce some concepts of cavity optomechanics which are useful for the understanding of Publication II, Publication III and Publication IV.

2. Elastic theory of a beam

In the 18^{th} century Leonhard Euler and Jacques Bernoulli derived the first theory for describing the deformation of a beam. It was only a century later that their theory was used and validated with the construction of the Eiffel tower. Since then this theory has been widely applied in the construction of many structures such as bridges and buildings and it is the same theory which describes the flexural vibrations of a nanoresonator. The purpose of this chapter is to present the necessary tools to understand the dependence of the vibration's eigenfrequency with the size of the resonator and to find out how a beam is coupled to an external force. I follow partially Refs. [15, 16, 17]. I start by deriving the potential energy of a slightly bent beam. Starting from the energy, I derive the Euler-Bernoulli equation whose solutions describe the flexural vibrations of the beam and show that the eigenfrequencies of the beam are inversely proportional to its size. Then I study a nonuniform resonator which consists of a resonator which displays a discontinuity in its physical properties. I demonstrate that at the point where the discontinuity occurs the slope, the moment and the force between the two parts of the resonator have to be equal. I then consider the case where one part of the beam is stiffer than the other one and show that in this case the eigenmodes of the beam are composed of the mode of a cantilever and a doubly clamped beam.

2.1 Bending energy

The bending energy is the energy stored in the beam when a torque (also called bending moment in beam theory) is applied to its end or when a load is applied perpendicularly to its axis. To derive its expression, let us consider an uniform beam which is slightly bent in the X, Z plane. The deformation of the beam from its unbent state is characterized by

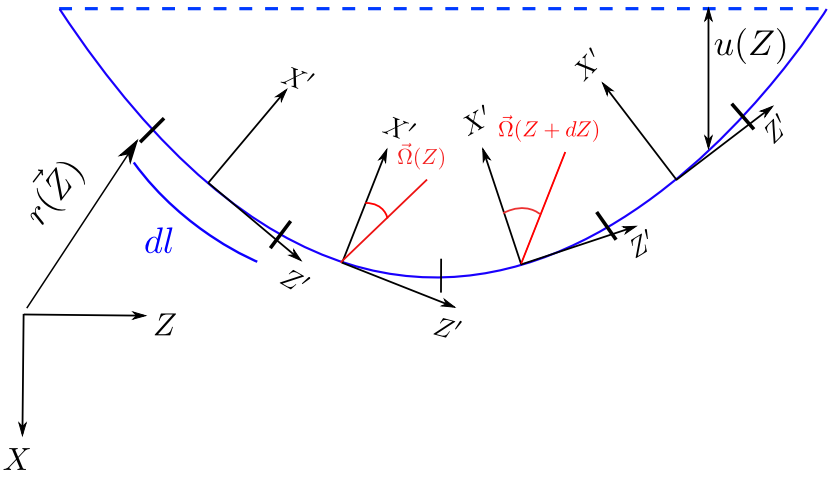

Figure 2.1. Schematic picture of the bent beam with $\vec{r}(Z)$ being the radius vector and $u(Z)$ the deformation of the beam from its unbent state. Upon the deformation each neighboring segment of the beam with lenght dl is rotated by an angle $\vec{\Omega}(Z)$.

the flexural deformation $u(Z)$. We divide the beam into small segments of length dl and attach to each of them a coordinate system X', Z'. We choose Z' such that it is aligned with the axis of each beam's element. We define $\vec{r}(Z)$ to be radius vector giving the position of the points on the beam and we define the unit tangent vector $\vec{t} = \frac{\vec{r}'(Z)}{|\vec{r}'(Z)|} = \frac{d\vec{r}}{dZ}\frac{dZ}{|d\vec{r}(Z)|} = \frac{d\vec{r}}{dl}$. As a result of the bending, each neighboring segment is rotated by an angle $\vec{\Omega}(Z)$ along the Y axis (see Fig. 2.1). Therefore the deformation is characterized by the variation of this angle $\vec{\Theta}$ between the two segments $\vec{\Theta}(Z) = \frac{d\vec{\Omega}(Z)}{dl}$. Assuming that the relative rotation $\vec{\Theta}(Z)$ between neighbouring segment is small, the bending energy per unit of length is

$$E_{\text{bending}} = \frac{1}{2}k\Theta(Z)^2, \tag{2.1}$$

where k is the spring's torsion coefficient and depends on the shape and material the beam is made of. This spring constant can be rewritten as $k = EI_y$ [17] where E is the Young modulus and represents the stiffness of the material and I_y is its bending moment. The latter is a geometry dependent coefficient and describes how the beam is deformed in the X direction. The aim now is to find an expression for $\vec{\Omega}(Z)$ as a function of the deformation $u(Z)$. We proceed as follows. On one hand, when moving from one segment of the beam to another, the variation of the tangent vector is $\frac{d\vec{t}}{dl}$ on the other hand the tangent vector is simply rotated by an angle $\vec{\Omega}(Z)$, thus

$$\frac{d\vec{t}}{dl} = \vec{\Theta}(Z) \times \vec{t}. \tag{2.2}$$

Taking the cross product of this equation with $\vec{t}$ and using $\vec{a} \times \vec{b} \times \vec{c} = (\vec{a} \cdot \vec{c})\vec{b} - (\vec{a} \cdot \vec{b})\vec{c}$, we obtain

$$\vec{\Theta}(Z) \quad = \quad \vec{t} \times \frac{d\vec{t}}{dl}. \tag{2.3}$$

Since the beam is slightly bent, one can approximate $dl \approx dZ$. In addition for small bending, the tangent vector $\vec{t}$ is almost parallel to the Z axis and the difference in direction can be neglected. Therefore

$$|\vec{\Theta}(Z)| = \frac{d^2u(Z)}{dZ^2}. \tag{2.4}$$

substituing this expression in Eq. (2.1) and defining $z = Z/L$ and $\langle v|w\rangle = \int_0^1 v(z,t)w(z,t)dz$. The energy of a beam of length L can be expressed as

$$E_{\text{bending}} \quad = \quad \frac{EI_y}{2L^3}\langle u''|u''\rangle, \tag{2.5}$$

where the prime denotes the derivative with respect to z. In the next section we investigate what happens when the bending becomes large and estimate the stress energy.

2.2 The stress energy

As the deformation increases, the beam stretches. As long as the amplitude of the deformation is smaller than the width of the beam this effect can be neglected. However, nanomechanical resonators can be strongly driven causing the amplitude of the vibrations to exceed the width of the resonator. Therefore, in addition to the bending energy one has to add the stress energy coming from the extension in the length ΔL of the beam

$$E_{\text{stress}} = \frac{1}{2}\frac{ES}{L}\Delta L^2, \tag{2.6}$$

where S denotes the beam's cross section. Upon the deformation $u(Z,t)$ (Fig. 2.2) the beam stretches to an amount given by

$$\Delta L = \int_0^L \sqrt{1 + \left(\frac{du(Z,t)}{dZ}\right)^2}\, dZ - L \simeq \frac{1}{2L}\langle u'|u'\rangle, \tag{2.7}$$

where we assumed $\left(\frac{du(Z,t)}{dZ}\right)^2 \ll 1$. Therefore the stress energy is

$$E_{\text{stress}} = \frac{ES}{8L^3}\langle u'|u'\rangle^2. \tag{2.8}$$

In addition to the stress coming from the deformation of the beam, we can also include an initial tension in the beam T_0 coming from its fabrication process. The corresponding energy is

$$E_{\text{tension}} = \frac{T_0}{2L}\langle u'|u'\rangle. \tag{2.9}$$

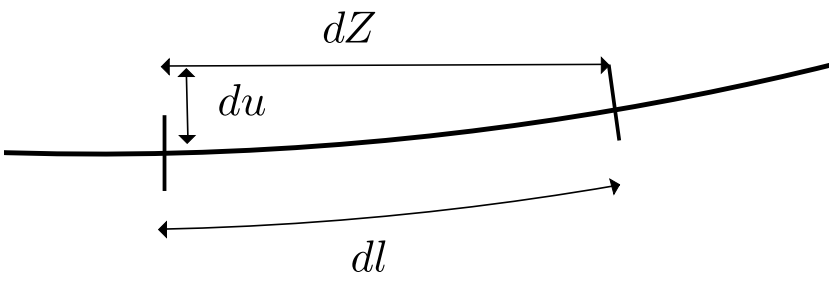

Figure 2.2. Schematic picture of the stretched beam.

The stress energy, the bending energy and the tension energy together form the mechanical potential energy of a beam whose deformation from its unbent state is given by $u(z,t)$.

2.3 Euler-Bernoulli equation.

We now describe the shape of the deformation $u(z,t)$. We start our discussion by considering a beam whose axis is along the z axis. It has a length L, mass m and cross section S. Let $V[u(z,t)]$ be the external potential of a force f acting on the beam which creates a deformation $u(z,t)$ from the unbent state of the beam. Using Eqs. (2.5), (2.8) and (2.9) the Lagrangian of the system is

$$\mathcal{L} = \frac{m}{2}\langle \dot{u}|\dot{u}\rangle - \frac{EI_y}{2L^3}\langle u''|u''\rangle - \frac{T_0}{2L}\langle u'|u'\rangle - \frac{ES}{8L^3}\langle u'|u'\rangle^2 - V[u(z,t)], \quad (2.10)$$

with $\dot{u} = \frac{du(z,t)}{dt}$. Solving $\delta S = \delta \int dt\mathcal{L} = 0$, with S being the action and δS being its functional derivative, the equation of motion for the flexural vibration $u(z,t)$ is

$$m\frac{d^2u(z,t)}{dt^2} + \frac{EI_y}{L^3}\frac{d^4u(z,t)}{dz^4} - \left[\frac{T_0}{L} + \frac{ES}{2L^3}\langle u'|u'\rangle\right]\frac{d^2u(z,t)}{dz^2} = f(z,t) \quad (2.11)$$

This equation is the Euler-Bernoulli equation. It is a fourth-order nonlinear differential equation and describes the deformation $u(z,t)$ of a beam. Solving this differential equation can be challenging due to the nonlinear term coming from the stress energy. To simplify this task we expand the deformation on the flexural eigenmodes of the beam. This method is known as the Galerkin method [18]. To find those eigenmodes we consider a beam without induced tension coming from the stress energy and in absence of an external force. Assuming a harmonic time dependence

$u(z,t) = e^{i\omega t}\chi(z)$ the deformation satisfies the eigenvalue equation

$$\frac{EI_y}{L^3}\frac{d^4\chi(z)}{dz^4} = m\omega^2\chi(z). \tag{2.12}$$

This equation looks similar to the harmonic oscillator equation but the significant difference is the presence of the fourth order derivative. It can be solved with $\chi(z) = e^{Kz}$ leading to

$$K = \pm\sqrt[4]{\pm\kappa} \tag{2.13}$$

$$\kappa = \frac{m\omega^2 L^3}{EI_y}. \tag{2.14}$$

Therefore the general solutions of the Euler-Bernoulli equation are

$$\chi(z) = Ae^{\kappa z} + Be^{-\kappa z} + Ce^{i\kappa z} + De^{-i\kappa x}, \tag{2.15}$$

or in terms of trigonometric and hyperbolic functions

$$\chi(z) = a\cos(\kappa z) + b\sin(\kappa z) + c\cosh(\kappa z) + d\sinh(\kappa z), \tag{2.16}$$

where a, b, c, and d are given by the boundary conditions which are imposed by the system we study. The most common systems encountered in nanomechanical systems are the doubly clamped beams and the cantilever, the latter consisting of a beam having one end clamped and the other free. In the following we only consider the doubly clamped beam. The treatment of the cantilever can be found in [17]. The doubly clamped beam has the boundary conditions

$$\chi(0) = \chi(L) = 0 \tag{2.17}$$

$$\chi'(0) = \chi'(L) = 0. \tag{2.18}$$

These boundary conditions imply that $a = -c$ and $b = -d$ and κ has discrete values $\kappa_1, \kappa_2, ..\kappa_n$ which have to satisfy

$$\cos(\kappa_n)\cosh(\kappa_n) - 1 = 0. \tag{2.19}$$

This equation can be solved numerically and leads to $\kappa_1 = 4.73$, $\kappa_2 = 7.85$, $\kappa_3 = 10.99$... The mode shapes $\chi_n(z)$ for the three lowest modes are plotted in Fig. 2.3. The corresponding eigenfrequencies are given by

$$\omega_n = \sqrt{\frac{EI_y}{\rho S}}\frac{\kappa_n}{L^2}, \tag{2.20}$$

where ρ is the mass density of the beam. Therefore the eigenfrequencies of the beam are inversely proportional to the size of the system.

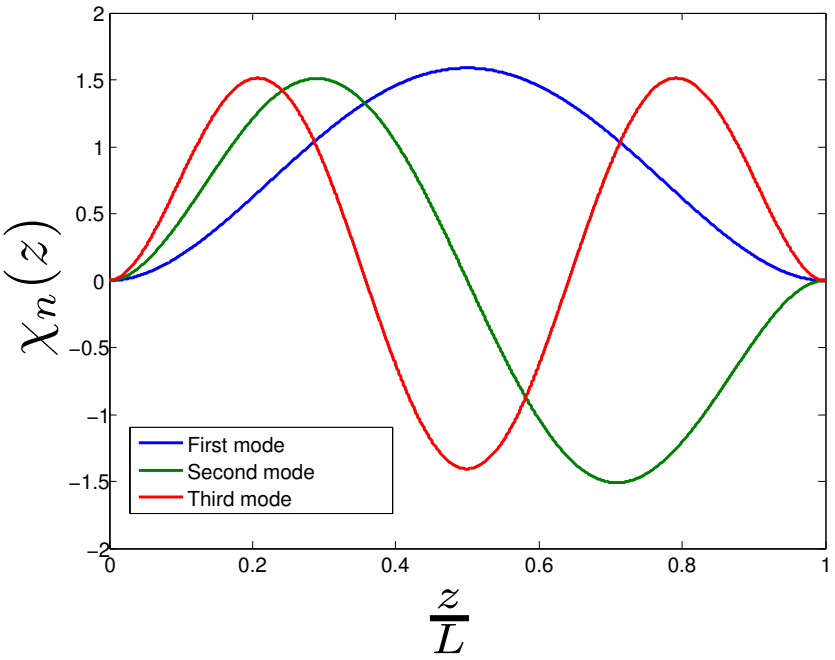

Figure 2.3. The three first mode shapes for a doubly clamped beam.

2.4 Nonuniform resonators

We now discuss how one can describe a nonuniform resonator which consists of a beam having an abrupt change in its physical properties, such as the mass density, the Young modulus etc. at some location. This kind of a resonator can be encountered in NEMS since the contacts holding the suspended resonator can be suspended themselves and thus be part of the vibrating system. For such a system the Euler-Bernoulli equation describing the flexural modes is

$$\frac{d^2}{dx^2}\left[\alpha(x)\frac{d^2u}{dx^2}\right] - \gamma(x)u = 0, \tag{2.21}$$

with $\alpha(x) = E(x)I(x)$ and $\gamma(x) = \rho(x)A(x)\omega^2$. For simplicity we suppose that there is only one discountinuity. In this case the resonator can be seen as a "beam composed of two beams". If we take the discountinuity in the physical properties to be at $x = 0$ we obtain

$$\alpha_l\frac{d^4u_l}{dx^4} - \gamma_l u_l = 0 \quad \text{for } x < 0, \tag{2.22}$$

$$\alpha_r\frac{d^4u_r}{dx^4} - \gamma_r u_r = 0 \quad \text{for } x > 0, \tag{2.23}$$

or in a more condensed way :

$$\Theta(-x)\left(\alpha_l\frac{d^4u_l}{dx^4} - \gamma_l\frac{d^2u_l}{dt^2}\right) + \Theta(x)\left(\alpha_r\frac{d^4u_r}{dx^4} - \gamma_r\frac{d^2u_r}{dt^2}\right) = 0, \tag{2.24}$$

with $\alpha_{l/r} = (EI)_{l/r}$ and $\gamma_{l/r} = (\rho A)_{l/r}$. The question we are asking now is what are the boundary conditions at $x = 0$ such that taking

$$u(x) = \Theta(-x)u_l(x) + \Theta(x)u_r(x), \tag{2.25}$$

$$\alpha(x) = \Theta(-x)\alpha_l + \Theta(x)\alpha_r, \tag{2.26}$$

$$\gamma(x) = \Theta(-x)\gamma_l + \Theta(x)\gamma_r, \tag{2.27}$$

and substituting these expressions in Eq. (2.21) we recover Eq. (2.24). Taking the first and second derivative of u we obtain

$$u'(x) = \Theta(-x)u_l'(x) + \Theta(x)u_r'(x) + (u_r(x) - u_l(x))\delta(x), \tag{2.28}$$

$$u''(x) = \Theta(-x)u_l''(x) + \Theta(x)u_r''(x) + (u_r'(x) - u_l'(x))\delta(x). \tag{2.29}$$

Therefore using the distribution product rules

$$\Theta(x)\Theta(x) = \Theta(x), \tag{2.30}$$

$$\Theta(x)\Theta(-x) = 0, \tag{2.31}$$

$$\delta(x)\Theta(\pm x) = \frac{1}{2}\delta(x), \tag{2.32}$$

we obtain for $\alpha(x)u''(x)$

$$\alpha(x)u''(x) = \alpha_l u_l''(x)\Theta(-x) + \alpha_r u_r''(x)\Theta(x) + \frac{1}{2}(\alpha_l + \alpha_r)(u_r'(x) - u_l'(x))\delta(x). \tag{2.33}$$

Taking the derivative of (2.33) we arrive at

$$\begin{aligned}(\alpha(x)u''(x))' &= \alpha_l u_l'''(x)\Theta(-x) + \alpha_r u_r'''(x)\Theta(x) \\ &+ (\alpha_r u_r''(x) - \alpha_l u_l''(x))\delta(x).\end{aligned} \tag{2.34}$$

Integrating Eq. (2.21) between ϵ and $-\epsilon$ and taking the limit $\epsilon \to 0$ we obtain

$$\begin{aligned}\lim_{\epsilon\to 0}\int_{-\epsilon}^{\epsilon}\gamma(x)u(x)\mathrm{dx} &= \lim_{\epsilon\to 0}\int_{-\epsilon}^{\epsilon}\frac{d^2}{dx^2}\left[\alpha(x)u''(x)\right]\mathrm{dx}, \\ &= \lim_{\epsilon\to 0}\left[(\alpha(x)u''(x))'\right]_{-\epsilon}^{\epsilon}, \\ 0 &= \alpha_r u_r'''(0) - \alpha_l u_l'''(0).\end{aligned}$$

Thus the first boundary condition is

$$\alpha_r u_r'''(0) = \alpha_l u_l'''(0). \tag{2.35}$$

In order to find the second boundary condition, we doubly integrate Eq. (2.21) and obtain

$$\lim_{\epsilon\to 0}\int_{-\epsilon}^{\epsilon}(\alpha(x)u''(x))' = \lim_{\epsilon\to 0}\int_{-\epsilon}^{\epsilon}\gamma U, \tag{2.36}$$

where U is the antiderivatives of u. Therefore using (2.34) one gets

$$\alpha_r u_r''(0) = \alpha_l u_l''(0). \tag{2.37}$$

In the same way defining U_2 the second antiderivative of u we get

$$\lim_{\epsilon \to 0} \int_{-\epsilon}^{\epsilon} (\alpha(x) u''(x)) = \lim_{\epsilon \to 0} \int_{-\epsilon}^{\epsilon} \gamma U_2 = 0, \tag{2.38}$$

and using (2.33) one obtains

$$u_r'(0) = u_l'(0). \tag{2.39}$$

Imposing that $u(x)$ is continuous at $x = 0$, the boundary conditions are

$$\begin{cases} u_r(0) & = & u_l(0) \\ u_r'(0) & = & u_l'(0) \\ \alpha_r u_r''(0) & = & \alpha_l u_l''(0) \\ \alpha_l u_r'''(0) & = & \alpha_l u_l'''(0). \end{cases}$$

Each of these conditions correspond to a physical quantity which has to be conserved at the discontinuity. The first condition is simply a continuity condition. The second assures that the slope of the beam on the left and right part of the discontinuity is the same. The third boundary condition makes sure that the torque between the left and the right part of the beam is the same and finally the last condition ensures that the force exerted at the discontinuity is equal on both sides. One interesting limit to consider is the case where one of the beams is stiffer than the other part. For $\alpha_l \gg \alpha_r$ which corresponds to the case where the left part of the resonator is stiffer than the right part, the flexural modes must satisfy

$$[1 + \cos(k_l L_l) \cosh(k_l L_l)] \, [1 - \cos(\epsilon k_r L_r) \cosh(k_r L_r)] = 0, \tag{2.40}$$

with $k_{l,r} = \sqrt{\gamma_{l/r}/\alpha_{l/r}}$ and $\epsilon = k_l/k_r$ and $L_{l/r}$ is the length of the left and right part or the beam. This equation is satisfied when k_r fulfills the doubly clamped beam eigenmode equation (Eq. 2.19) or when k_l satisfies the eigenmode equation of a cantilever [17]. In Fig. 2.4 the four first modes of a nonuniform beam with $\frac{\alpha_r}{\alpha_l} = 10^{-3}$, $L_l = L_r = L$ and $k_l/k_r = 1$ are presented. We remark that the second, third and fourth mode are in fact composed of a mode of a cantilever (on the left side) and a mode of a doubly clamped beam (on the right side).

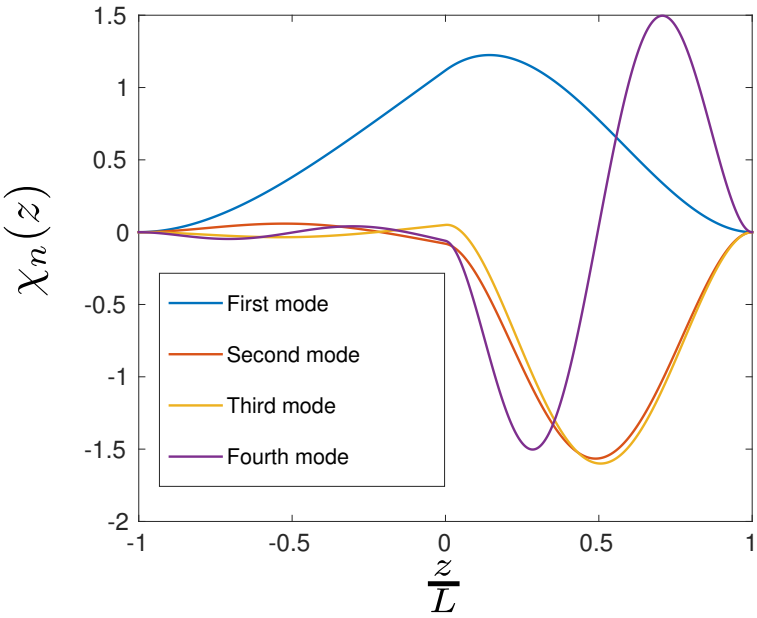

Figure 2.4. Plot of the first four modes $\chi(z)$ of a nonuniform beam with $\frac{\alpha_r}{\alpha_l} = 10^{-3}$, $L_l = L_r = L$ and $k_l/k_r = 1$. For the first mode $Lk_l = 1.88$, for the second mode $Lk_l = 4.65$, for the third mode $Lk_l = 4.78$ and for the fourth mode $Lk_l = 7.79$.

3. Nonlinear dynamics

In the previous chapter we solve the Euler-Bernoulli equation but neglect the nonlinear term coming from the large deformation: the induced tension. In many experiments the effect of this nonlinear term can be observed [19, 20, 21]. The nonlinear effects of the induced tension manifest themselves for example in the frequency at which the resonator vibrates and by exhibiting nonlinear dynamics (see Fig. 3.1). Consequently it is important to understand the nonlinearities either to avoid them [22] or on the contrary to exploit them [23, 24]. In this chapter we derive the nonlinearities which arise from the induced tension. We then discuss what their effects on the frequency are and the equation of motion of the flexural mode. Especially we demonstrate that in the presence of induced tension the frequency increases in systems which allow large deformation before decreasing because of the nonlinearity coming from an external potential. In addition we show how the induced tension makes the frequency response function dependent on the amplitude of the vibrations. Finally we discuss how the nonlinearity can be used for observing macroscopic quantum tunneling.

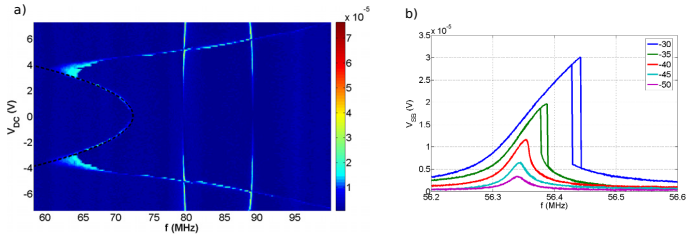

Figure 3.1. a) Mechanical resonance frequency as a function of a DC gate voltage of a graphene based resonator with length $L = 1\,\mu\mathrm{m}$ and width $W = 1\,\mu\mathrm{m}$. b) Response function of a graphene based resonator with length $L = 1.5\,\mu\mathrm{m}$ and width $W = 2\,\mu\mathrm{m}$ with a drive power stepped from $-50\,\mathrm{dBm}$ to $-30\,\mathrm{dBm}$. The color scale gives the amplitude of the signal in Volt. Courtesy of Xuefeng Song, Aalto University.

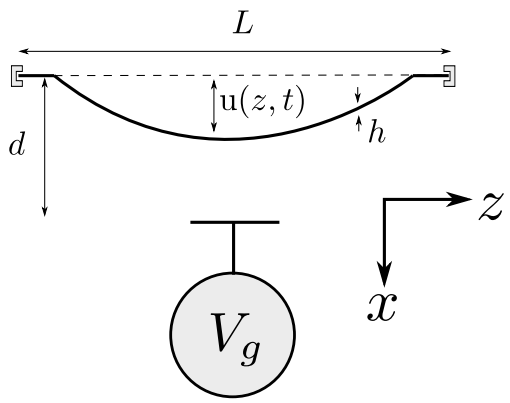

Figure 3.2. Schematic picture of the system which consist of doubly clamped beam with length L, width w and thickness h whose deformation is controlled by a gate voltage V_g.

3.1 Tension induced nonlinearities

As discussed in the previous section, for large deformations, an additional term appears in the Euler-Bernoulli equation to take into account the tension which builds up in the beam. Let us consider a rectangular resonator of length L, width w, thickness h and cross section $S = wh$. The resonator has a bending moment I_y and is made of a material whose Young modulus is E. We study a typical case where an electrostatic force created by a gate voltage V_g situated at a distance d from the beam induces a deformation $\mathrm{u}(z,t)$ as depicted in Fig. 3.2. Therefore the potential energy of the force acting on the beam is

$$V[\mathrm{u}(z,t)] = -\frac{{V_g}^2}{2}\int_0^1 C[1-\frac{\mathrm{u}(z,t)}{d}]dz, \tag{3.1}$$

where C is the function describing the capacitance between the gate and the beam. Scaling the deformation with the distance between gate and beam d, $\mathrm{u}(z,t) = d\,u(z,t)$ the potential energy of the system is

$$E_{\text{potential}} = \\ \frac{1}{2}m\omega_0^2 d^2\langle u''|u''\rangle + \frac{1}{2}m\omega_s^2 d^2\left[\tau_0 + \langle u'|u'\rangle\right]\langle u'|u'\rangle - \frac{{V_g}^2}{2}\int_0^1 C[1-u(z,t)]dz, \tag{3.2}$$

with $m\omega_0^2 = \frac{EI_y}{L^3}$, $m\omega_s^2 = \frac{ESd^2}{4L^3}$ and $m\omega_s^2\tau = \frac{T_0}{L}$. Let us assume that $u(z,t)$ is the sum of a static deformation $u_0(z)$ given by solving $\frac{dE_{\text{potential}}}{du} = 0$ and a small time varying deformation $u_1(z,t) \ll u_0(z)$ which oscillates around the equilibrium solution $u_0(z)$. In order to simplify the analysis, we ex-

pand the deformation as $u_1 = \sum_n x_n(t)\chi_n(z)$ with $\chi_n(z)$ as the mode shape of the deformation given by the eigenmode of a doubly clamped beam and x_n as the amplitude of the deformation in the eigenmode n. Substituting $u_1 = \sum_n x_n(t)\chi_n(z)$ in Eq. (3.3), the potential energy becomes

$$\frac{E_{\text{potential}}}{m\omega_s^2 d^2} = \frac{1}{2}[\Omega^2]^n_m x^m x_n + \mathcal{T}^n_{mo} x_n x^m x^o + \mathcal{F}^{no}_{mp} x_n x_o x^m x^p + \mathcal{O}(x^5). \quad (3.3)$$

with

$$\begin{aligned}
[\Omega^2]^n_m &= \frac{\omega_0^2}{\omega_s^2}\langle\chi_n''|\chi_m''\rangle + [(\tau_0 + 2\langle u_0'|u_0'\rangle)\langle\chi_n'|\chi_m'\rangle + 4\langle\chi_n'|u_0'\rangle\langle u_0'|\chi_m'\rangle] \\
&- \frac{V_g^2}{2m\omega_s^2 d^2}\int_0^1 \frac{d^2C[1-u_0]}{du_1^2}\chi_n(z)\chi_m(z)dz. \quad (3.4) \\
\mathcal{T}^n_{mo} &= 2\langle u_0'|\chi_o'\rangle\langle\chi_n'|\chi_m'\rangle \\
&- \frac{V_g^2}{12m\omega_s^2 d^2}\int_0^1 \frac{d^3C[1-u_0]}{du_1^3}\chi_n(z)\chi_m(z)\chi_o(z)dz. \quad (3.5) \\
\mathcal{F}^{no}_{mp} &= \frac{1}{2}\langle\chi_n'|\chi_m'\rangle\langle\chi_o'|\chi_p'\rangle \\
&- \frac{V_g^2}{48m\omega_s^2 d^2}\int_0^1 \frac{d^3C[1-u_0]}{du_1^3}\chi_n(z)\chi_m(z)\chi_o(z)\chi_p(z)4dz. \quad (3.6)
\end{aligned}$$

These coefficients describe how each mode is coupled to each other. Ω^2 determines the eigenfrequecies at which the beam vibrates. The second term of Eq. (3.4) contains contributions coming from the initial and induced tension and the last term shows the effect of the electrostatic force. $\mathcal{T}$ is a nonlinear coefficient which originates from the asymmetry of the system, the first term describes the effect of the static deformation and the second term is the effect coming from the electrostatic force. $\mathcal{F}$ is known as the Duffing nonlinear coefficient [25, 26]. The first term is purely a geometric constant which depends on the mode we are considering and the second term is the contribution from the electrostatic force. These nonlinearities can be used to detect the motion of one mode by measuring another mode as in [27, 28]. In the following sections we focus on the self-nonlinearity by setting $n = m = o = p$.

3.2 Effect of tension on the eigenfrequency

The eigenfrequency of the flexural mode are given by (3.4). The third and fourth terms of this equation originate from the induced tension. In order to understand how they alter the frequency it is necessary to find the equilibrium solution $u_0(z)$. For simplicity we assume a low gate voltage such that $u_0 \ll 1$. The equilibrium position is given by

$$\frac{\omega_0^2}{\omega_s^2}u_0''''(z) - \tau u_0''(z) = V^2, \quad (3.7)$$

where $V^2 = \frac{V_g^2}{2m\omega_s^2 d^2}\frac{dC[1]}{du}$ and where we defined the dimensionless total tension

$$\tau = \tau_0 + 2\langle u_0' | u_0' \rangle. \tag{3.8}$$

For a doubly clamped beam, the solution of (3.7) is [29]

$$u_0 = \frac{V^2}{2\tau\xi}\left[\xi(1-x)x + \coth\left(\frac{\xi}{2}\right)(\cosh(\xi x) - 1) - \sinh(\xi x)\right] \tag{3.9}$$

with $\xi = \sqrt{\tau\omega_s^2/\omega_0^2}$. Substituting Eq. (3.9) into Eq. (3.8) we obtain the self-consistency equation for the tension

$$\tau = \tau_0 + \frac{V^4}{6\tau^2\xi^2}\left(\xi^2 + 24 - \frac{3\left(\xi^2 + 3\xi\sinh(\xi)\right)}{\cosh(\xi) - 1}\right). \tag{3.10}$$

A characteristic voltage can be found from Eq. (3.10). Substituting $\tau \equiv \tau_0$ and comparing τ_0 to the second term on the right hand side of the equation gives the threshold voltage $\tilde{V}$ under which the initial tension τ_0 is large compared to the tension built via the deformation. This voltage is

$$\tilde{V}^4 = \frac{6\tau_0^4}{\frac{24}{\tau_0}\frac{\omega_0^2}{\omega_s^2} - \frac{3+\frac{9}{\sqrt{\tau_0}}\sqrt{\frac{\omega_0^2}{\omega_s^2}}\sinh\left(\sqrt{\tau_0\frac{\omega_s^2}{\omega_0^2}}\right)}{\cosh\left(\sqrt{\tau_0\frac{\omega_s^2}{\omega_0^2}}\right)-1}} \tag{3.11}$$

Above this voltage the tension mainly comes the deformation of the beam. There are two particular regimes to study. The first regime corresponds to the situation where the beam is sligthly bent and $\omega_0^2/\omega_s^2 \gg \tau$. Consequently the bending energy is small compared to the stress energy and the induced tension becomes [29]

$$\tau = \frac{V^4}{15120}\frac{\omega_s^2}{\omega_0^2}. \tag{3.12}$$

The second regime is the opposite limit when the beam undergoes a large deformation $\frac{\omega_0^2}{\omega_s^2} \ll \tau$. In this case [29]

$$\tau = \frac{V^{4/3}}{6^{1/3}}. \tag{3.13}$$

We can now sketch the behavior of the eigenfrequencies of the flexural modes, as a function of the voltage, by substituting Eq. (3.12) and Eq. (3.13) in Eq. (3.4). For $\omega_0^2/\omega_s^2 \gg \tau$, i.e., in the regime where the bending energy is larger than the induced tension energy the change in the frequency is essentially coming from the electrostatic energy, thus the behavior of the frequency is $\propto -V_g^2$, decreasing as the voltage increases. In the opposite regime, $\omega_0^2/\omega_s^2 \gg \tau$, at first the eigenfrequency decreases until $V = \tilde{V}$ above which it behaves $\propto V^{4/3}$ and increases. In Fig. 3.3, the eigenfrequency of the first flexural mode is plotted as a function of the voltage by numerically solving the Euler-Bernoulli equation with a parallel-plate model capacitor $C[1-u_0] = \frac{\epsilon w L}{d(1-u(x,t))}$.

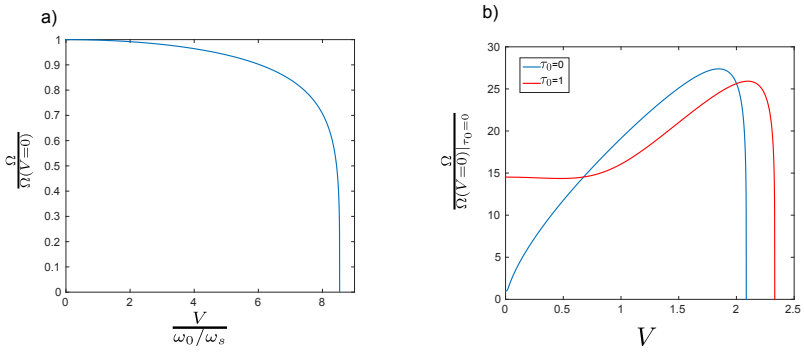

Figure 3.3. Behavior of the frequency of the first mode as a function of $V = \sqrt{\frac{V_g^2}{2m\omega_s^2 d^2}\frac{dC[1]}{du}}$. a) Frequency of the first mode in the weak bending regime $\omega_0^2 \gg \omega_s^2$. b) Frequency of the first mode in the strong bending regime $\omega_s^2 \gg \omega_0^2$ with and without initial tension τ_0.

3.3 Pull-in Effect and Macroscopic Quantum Tunneling.

In the previous section we limit the study for low gate voltage such that $u(x,t) \ll 1$. However, as the gate voltage V increases, the deformation becomes larger until the resonator is pulled into contact with the gate at $V = V_c$. This effect manifests itself by the frequency quickly tending to zero when the critical voltage is reached as shown in Fig. 3.3. From an energy point of view what happens is that when increasing the voltage the minimum of the potential energy becomes metastable and disappears at $V = V_c$ as depicted in Fig. 3.4 . An estimation of this critical voltage can be found using Eq. (3.3). To obtain a simple analytical value, we assume that $u(z,t) = x\chi(z)$ and choose, as a model for the capacitance: a parallel plate model which simply depends on the amplitude x of the deformation instead of the full shape of the defomation $u(x)$. In order to find the critical voltage one needs to solve the system

$$\frac{dE_{\text{potential}}}{dx} = 0, \tag{3.14}$$

$$\frac{d^2E_{\text{potential}}}{dx^2} = 0. \tag{3.15}$$

The first equation gives the equilibrium amplitude x_0 at which the resonator vibrates and the second equation is the frequency of the vibrations which is 0 when the resonator pulls into contact with the gate. Expanding up to the third order for a small variation around the equilibrium amplitude x_0 we obtain

$$\frac{E_{\text{potential}}}{m\omega_s^2 d^2} = \frac{1}{2}\Omega^2 x^2 + \alpha x^3 \tag{3.16}$$

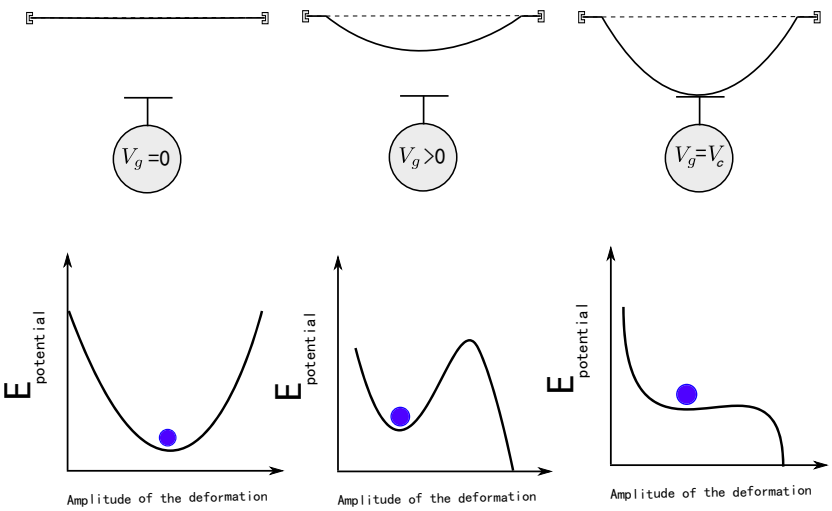

Figure 3.4. Schematic picture of the potential energy of the mechanical resonator. As the gate voltage increases the minimum of the potential energy becomes metastable until it disappears for $V = V_c$.

with

$$\Omega^2 = \frac{\omega_0^2}{\omega_s^2}\langle\chi''|\chi''\rangle + \tau_0\langle\chi'|\chi'\rangle + 3\langle\chi'|\chi'\rangle^2 x_0^2 - \frac{V^2}{(1-x_0)^3} \tag{3.17}$$

$$\alpha = 2x_0\langle\chi'|\chi'\rangle^2 - \frac{V^2}{(1-x_0)^4}. \tag{3.18}$$

Hence for $\omega_0^2/\omega_s^2 \gg \tau$ the critical voltage is $V_c = \frac{2}{3}\sqrt{\frac{\langle\chi''|\chi''\rangle}{3}}\frac{\omega_0}{\omega_s}$ [30] while for $\omega_0^2/\omega_s^2 \ll \tau$ the critical voltage is $V_c = \frac{6}{25}\sqrt{\frac{6}{5}}\langle\chi'|\chi'\rangle$. Comparing these estimations with the numerical values found in Fig. 3.3 we find that for the first mode $\langle\chi''|\chi''\rangle = 500.8$ and consequently we find that $V_c = 8.6\frac{\omega_0}{\omega_s}$ which is in agreement with the numerical result while for the $\omega_0^2/\omega_s^2 \ll \tau$ we obtain for the first mode $\langle\chi'|\chi'\rangle = 12.3$ and $V_c = 3.2$ which over estimates the actual pull-in voltage. This error originates from the approximation we made of the capacitance.

In Publication I, we showed that the beam can be pulled into contact with the gate before the voltage reaches V_c by leaving the metastable minimum via quantum tunneling, the tunneling rate being given by [31] $\Gamma_Q = \omega_Q \exp[-18/5\frac{N}{\pi}]$, where $N = \frac{\Delta V}{\hbar\omega_s\Omega}$ is the number of states in a potential of height ΔV, $\omega_Q = 6\omega_s\Omega\sqrt{6N/\pi}$ and $\Omega = \Omega_n^n$. However at a temperature T the beam can also escape the metastable minimum via thermal activation, the rate being given by the Arrhenius law $\Gamma_T = \omega_s\Omega/(2\pi)\exp[-\Delta V/(k_bT)]$. These two mechanisms are competing as depicted in Fig. 3.5. The temperature from which the quantum tunneling dominates over the thermal

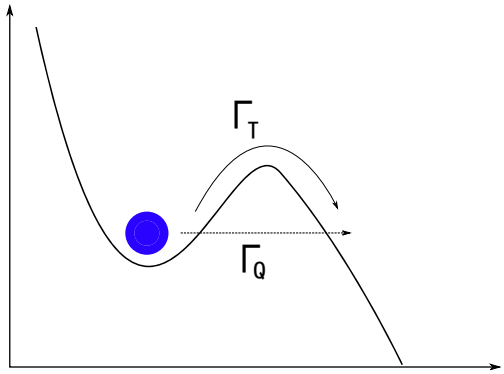

Figure 3.5. Schematic picture of the two physical processes involved in the escape from the metastable minimun.

escape is given by

$$T_Q = \frac{5}{36}\frac{\hbar\omega_s}{k_b}\Omega\frac{1}{1-\frac{5}{36}\ln\left(12\sqrt{\frac{6}{\pi}N}\right)}. \tag{3.19}$$

In addition, to maximize the quantum tunneling rate, the number of states N in the metastable minimum need to be small. The latter is given by

$$\begin{aligned} N &= \frac{\Delta V}{\hbar\omega_s\Omega} \\ &= \frac{m\omega_s d^2}{\hbar}\frac{\Omega^5}{54\alpha^2}. \end{aligned} \tag{3.20}$$

Therefore one needs to be close to the pull-in point since ΔV and consequently N is small. Having a high crossover temperature and having a small number of states is difficult to satisfy simultaneously since a high frequency is demanded to maximize the crossover temperature T_Q and at the same time, to obtain a sufficient quantum tunneling rate, one needs to be close to the pull-in point where the frequency is low. In Publication I we demonstrated that good candidates for observing macroscopic quantum phenomena are systems with low mass, high Young modulus and large ratio ω_s/ω_0. Materials such as carbon nanotubes or graphene fulfill these attributes.

3.4 Duffing nonlinearity.

In addition to altering the eigenfrequencies of the flexural mode, the induced tension is also adding two nonlinear terms, known as Duffing nonlinearities, making the potential energy quartic in the amplitude x (Eq. (3.2))

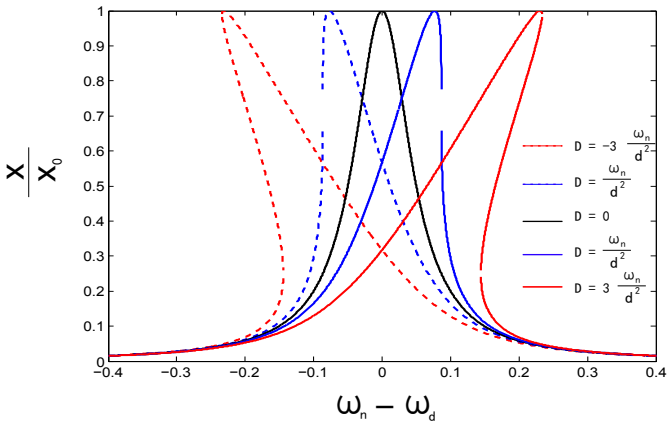

Figure 3.6. Behavior of the frequency response with $|f|^2 = \frac{8\gamma^3}{6\sqrt{3}\omega_n}d^2$ and $|x_0|^2 = 4\frac{|f^2|}{\gamma^2|d\omega_n|^2}$.

.

. When driving the system with a sinusoidal force with frequency ω_d and amplitude f_0 and including dissipation the equation of motion for the amplitude x is

$$\ddot{x} + \gamma\dot{x} + \omega_s^2\Omega^2 x + 3\frac{\omega_s^2}{d}\mathcal{T}x^2 + 4\frac{\omega_s^2}{d^2}\mathcal{F}x^3 = \frac{f_0}{d}\cos(\omega_d t), \tag{3.21}$$

where γ is the damping rate. The response function of Eq. (3.21) is

$$|x|^2 = \frac{|f_0/(d\omega_n)|^2}{(\omega_n - \omega_d - \frac{3}{8}\frac{D}{\omega_n}|x|^2)^2 + \left(\frac{\gamma}{2}\right)^2} \tag{3.22}$$

with $\omega_n = \omega_s\Omega$, $D = \frac{\omega_s^2}{d^2}\left(4\mathcal{F} - 10\left[\frac{\mathcal{T}}{\omega_n}\right]^2\right)$. The presence of the cubic nonlinearity $\mathcal{T}$ adds to the regular Duffing nonlinearity. Because $\mathcal{T}$ depends on the static deformation, it allows to tune the total nonlinear coefficient as discussed in Publication II. The response function (3.22) is plotted in Fig. 3.6. It depends on the amplitude of the deformation. When the deformation increases the resonance peak starts to lean toward higher frequencies when $D > 0$ and to lower frequencies when $D < 0$. Above a critical drive $\frac{|f_c|^2}{|d\omega_n|^2} = \frac{8\gamma^3}{9\sqrt{3}D/\omega_n}$, three different solutions appear for the amplitude among which two are stable and are situated at the lower and upper branches while the solution on the middle branch is unstable. In this region the value of the amplitude x depends on the history of the system. For example when sweeping the frequency upward the amplitude increases until it reaches the end of the upper branch at which point the amplitude jumps to the lower branch, and vice versa.

To summarize, we have derived the potential energy of a nanomechanical resonator driven by a nearby gate voltage. Taking into account the in-

duced tension we showed how the latter alters the eigenfrequency of the flexural mode. In addition we derived the Duffing nonlinearity and we find that a third-order nonlinearity related the a static deformation of the beam allow to tune the Duffing constant. In addition to the induced tension we also dicussed about nonlinearity coming from the external drive, namely the pull-in effect and how this nonlinear behaviour can be use for observing Macroscopic Quantum Tunneling.

4. Circuit optomechanics

Cavity optomechanics offers the opportunity to study the interaction between photons and a mechanical system. This field has gotten a great peak of interest with the demonstration of laser cooling of mechanical motion and sensitive displacement detection [9, 32, 33]. A typical system consists of a driven optical cavity whose one end is made of a vibrating mirror [34, 35] or can be a microwave cavity coupled to a mechanical resonator (see Fig 4.1). In both cases the eigenfrequency of the cavity depends on the vibration of the mechanical part, the vibration being created by a light-induced force: the radiation pressure force [36]. In this section I follow partially [37]. First we show how the radiation pressure coupling g arises in a system composed of a microwave cavity coupled to a mechanical resonator. We derive the Hamiltonian and show how the mechanical vibrations alter the frequency of the microwave cavity. Then we demonstrate how the radiation pressure can be used for cooling/heating the resonator to the ground state and show that the cooling/ heating is proportional g^2. We then discuss how one can improve the coupling g by coupling the cavity and the mechanical resonator to a single-Cooper pair transistor. Finally I discuss about a cross-Kerr nonlinearity which couples the number of phonons in the resonator to the number of photons in the cavity presented in Publication IV.

4.1 Radiation pressure

We consider a setup where the mechanical resonator is coupled to a microwave cavity driven by an external drive. The simplest model for this system is an LC resonator with inductance L and capacitance $C_0 + C_m(x)$, whose eigenfrequency is modulated by the amplitude of vibration x of the resonator. In addition the cavity is coupled capacitively through C_c to

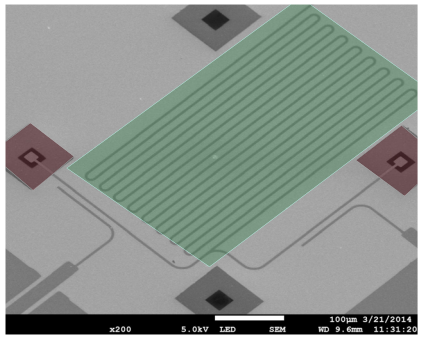

Figure 4.1. Microwave cavity (in green) coupled to two silicon nitride mechanical resonators (in red). Courtesy of Matthias Brandt, Aalto University.

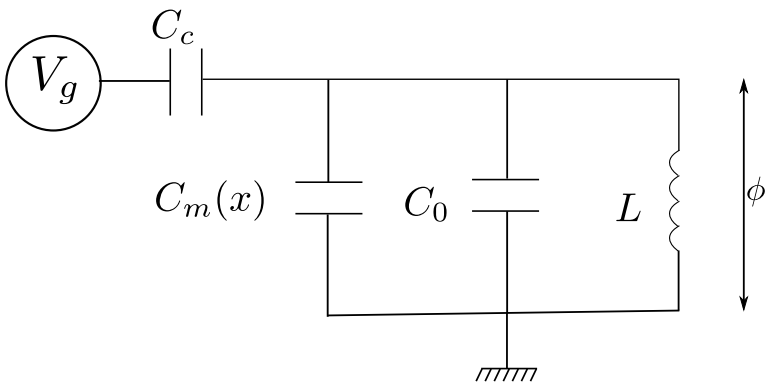

Figure 4.2. Equivalent circuit model of the microwave cavity. A LC resonator with inductance L and capacitance $C_0 + C_m(x)$. The mechanical resonator is taken into account via the capacitance $C_m(x)$ that depends on the amplitude x of vibrations.

driving a voltage $V_g(t) = V\cos(\omega_d t)$. The phase across the LC resonator is ϕ. The equivalent circuit model is sketched in Fig. 4.2. The Lagrangian of the electric circuit is

$$\mathcal{L}_c = \frac{1}{2}(C_0 + C_m(x))\dot{\phi}^2 + \frac{1}{2}(\dot{\phi} - V(t))^2 C_c - \frac{\phi^2}{2L}. \tag{4.1}$$

From the Lagrangian we obtain for the conjugate charge

$$q = \frac{\partial \mathcal{L}}{\partial \dot{\phi}} = (C_0 + C_m(x) + C_c)\dot{\phi} - C_c V. \tag{4.2}$$

Therefore the Hamiltonian of the total system consisting of the microwave cavity and the mechanical resonator is

$$\mathcal{H} = \frac{p^2}{2m} + \frac{m\omega_m^2}{2}x^2 + \frac{q^2}{2[C_c + C(x)]} + \frac{\phi^2}{2L} - q\frac{C_c V(t)}{C_c + C(x)}, \tag{4.3}$$

with m being the mass of the mechanical resonator and ω_m being the frequency of the mode at which the resonator vibrates and $C(x) = C_m(x) +$

C_0. The last term of Eq. (4.3) is the energy of the driving force. The quantum description is found with the usual canonical transformations

$$\phi = \sqrt{\frac{\hbar}{2}\sqrt{\frac{L}{[C_c + C(x)]}}}(a^\dagger + a), \tag{4.4}$$

$$q = i\sqrt{\frac{\hbar}{2}\sqrt{\frac{[C_t + C(x)]}{L}}}(a^\dagger - a), \tag{4.5}$$

$$x = \sqrt{\frac{\hbar}{2m\omega_m}}(b^\dagger + b), \tag{4.6}$$

$$p = i\sqrt{\frac{\hbar m\omega_m}{2}}(b^\dagger - b). \tag{4.7}$$

Therefore for $x \ll d$, with d being the distance between the gate and the resonator, and taking only into account the lowest order term in the force, i.e., neglecting the effect of the vibrations on the force (last term of Eq. (4.3)), the Hamiltonian of the system including the mechanical resonator is

$$\hbar\omega_c a^\dagger a + \hbar\omega_m b^\dagger b - \hbar g a^\dagger a(b^\dagger + b) - i\hbar f\cos(\omega_d t)(a^\dagger - a). \tag{4.8}$$

Here the cavity frequency $\omega_c = \frac{1}{\sqrt{L(C_c+C(0))}}$, the amplitude of the drive $f_p = \sqrt{\frac{\omega_c}{\hbar}}\frac{C_c}{\sqrt{C_c+C(0)}}V$ and $g = \frac{\omega_c}{2[C_c+C(0)]}\sqrt{\frac{\hbar}{2m\omega_m}}\frac{\partial C}{\partial x}$ is the radiation pressure coupling. The latter is a nonlinear coupling between the number of photons in the cavity and the amplitude of vibrations x of the mechanical resonator. However this coupling is usually small, for example in [38] $g = 40\,\mathrm{Hz}$ while $\omega_c/(2\pi) = 7\,\mathrm{GHz}$. Consequently the effect of the radiation pressure should not be observable. To bypass the weakness of the radiation pressure coupling a strong drive is applied to the cavity which shifts the number of photons in the cavity to a mean cavity photon number $|\alpha|^2$. As a result one can obtain a larger effective coupling $G = g|\alpha|^2$ at the cost of losing the nonlinear property of the interaction. Indeed using the input-output formalism [39] and assuming that $\omega_d = \omega_c + \Delta$ we obtain for the equation of motion

$$\dot{a} = -i[-\Delta + g(b^\dagger + b)]a - \frac{\kappa}{2}a - \frac{f_p}{2}, \tag{4.9}$$

$$\dot{b} = -i\omega_m b + iga^\dagger a - \frac{\gamma}{2} + \sqrt{\gamma}b_{in}, \tag{4.10}$$

where κ is the linewidth of the cavity and γ is the linewidth of the mechanical resonator. Here we have written the cavity operator a in a frame rotating with frequency ω_d and neglected the counter rotating term. We define b_{in} to be a small noise term acting on the mechanical resonator, κ

to be the damping rate of the cavity and γ the damping rate of the mechanical resonator. As mentioned above the effect of the drive is to induce a finite average number of photons in the cavity. Therefore we split the cavity and the mechanical operator into a sum of a coherent part originating from the coherent drive and a fluctuation part coming from the noise term, i.e., $a \equiv \alpha + \delta a$ and $b \equiv \beta + \delta b$. With this approximation the solutions for the coherent parts are

$$\alpha = \frac{-f/2}{\frac{\kappa}{2} - i[-\Delta - g(\beta^* + \beta)]} \tag{4.11}$$

$$\beta = \frac{ig^2|\alpha|^2}{\frac{\gamma}{2} + i\omega_m}. \tag{4.12}$$

The equations of motion for the fluctuations in the Fourier space are

$$[\frac{\kappa}{2} - i(\omega + \Delta)]\delta a = iG(\delta b^\dagger + \delta b) \tag{4.13}$$

$$[\frac{\gamma}{2} - i(\omega - \omega_m)]\delta b = iG(\delta a^\dagger + \delta a) + \sqrt{\gamma} b_{in}. \tag{4.14}$$

Here $\delta a(\omega) = \int_{-\infty}^{\infty} \delta a(t) e^{i\omega t}$ is the Fourier transform of δa and a similar definition is used for δb. We also define the effective radiation pressure coupling $G = g|\alpha|$ which is proportional to the number of photons pumped into the cavity. Although we lose the nonlinear character of the radiation pressure coupling, the linearized equation describes interesting phenomena such as ground state cooling and heating which are discussed in the next section.

4.2 Cooling and heating.

When driving the cavity with a frequency ω_d, as a consequence of the radiation pressure coupling, the vibrations of the resonator produce sideband peaks at $\omega_d \pm \omega_m$. The photons in these sidebands originate from inelastic (Raman) scattering and give the possibility to exchange energy between the resonator and the cavity when the drive is optimally detuned with $\Delta \approx \pm\omega_m$. For $\Delta = \omega_m$ the photons are preferably down-converted to ω_c and therefore the scattering process is accompanied with the excitation (heating) of the mechanical resonator, the system is in the blue sideband regime. For $\Delta = -\omega_m$ the photons are preferably up converted to ω_c thus the scattering process is accompanied with de-excitation (cooling) of the resonator, the system is in the red sideband regime. These processes are depicted in Fig. 4.3. In order to see the effect of the mechanical vibrations let us assume that the term b_{in} corresponds to a thermal drive which satisfies $\langle b_{in} \rangle = 0$ and $\langle b_{in}^\dagger(t') b_{in}(t) \rangle = n^{th}\delta(t' - t)$, where n^{th} is the number of

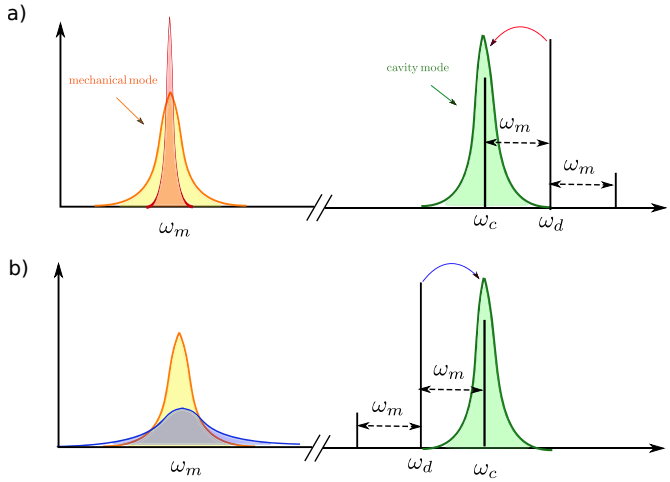

Figure 4.3. Schematic picture of the cooling and heating processes. a) Heating process: the energy is transfered from the cavity to the mechanical resonator. b) Cooling process: the energy is transfered from the mechanical resonator to the cavity.

phonons in the thermal bath damping the mechanical resonator. Solving for $\delta a^\dagger$, we find the response function F for the thermal input $\delta b_{in}^\dagger$ and obtain

$$F = G\sqrt{\gamma}\frac{{}^{[\frac{\gamma}{2}-i(\omega+\omega_m)]}/_{(\Delta-\omega-i\frac{\kappa}{2})}}{\left[(\frac{\gamma}{2}-i\omega)^2+\omega_m^2+\frac{4G^2\Delta\omega_m}{\Delta^2-(\omega+i\frac{\kappa}{2})^2}\right]}. \tag{4.15}$$

This frequency response function describes a Lorentzian whose resonance peak is around an effective frequency $\omega_m + \omega_{\text{shift}}$ with

$$\omega_{\text{shift}} = -\frac{G^2(\Delta^2-\omega_m^2+\frac{\kappa^2}{4})}{\omega_m}\left[\frac{1}{\frac{\kappa^2}{4}+(\omega_m+\Delta)^2}-\frac{1}{\frac{\kappa^2}{4}+(\omega_m-\Delta)^2}\right], \tag{4.16}$$

and whose linewidth is $\gamma_{\text{eff}} = \gamma + \Gamma_{\text{opt}}$ with

$$\Gamma_{\text{opt}} = G^2\kappa\left[\frac{1}{\frac{\kappa^2}{4}+(\omega_m+\Delta)^2}-\frac{1}{\frac{\kappa^2}{4}+(\omega_m-\Delta)^2}\right]. \tag{4.17}$$

For simplicity we assume below that we are in the fully sideband resolved limit $\omega_m \gg \kappa$. In addition $|\Delta| = |\omega_m|$ in which case Eqs. (4.16) and (4.17) are reduced to [37, 40]

$$\omega_{\text{shift}} = \mp\frac{G^2}{\omega_m} \tag{4.18}$$

$$\Gamma_{\text{opt}} = \pm\frac{4G}{\kappa} \tag{4.19}$$

where the upper sign corresponds to the red sideband ($\Delta = -\omega_m$) and the lower sign corresponds to the blue sideband ($\Delta = \omega_m$). In the case of the red detuning, $\Delta = -\omega_m$ the effective damping increases which permits to

cool the mechanical mode to its ground state [9, 41, 42]. In the case of the blue detuning we have the opposite effect and the effective damping decreases. The decreasing damping leads to heating of the mechanical resonator and, when the effective damping is zero, to a parametric instability [43] and can used for signal amplification [38].

4.3 Strong coupling regime

When one starts to increase the number of photons in the cavity it leads to an enhancement of the effective radiation pressure coupling $G = g\alpha$. At first this is just improving the cooling , since $\Gamma_{opt} \propto G$, until the coupling is strong enough so that the mechanical and cavity modes δb and δa hybridize. The simplest way to understand this phenomenon is to consider Eqs. (4.13) and (4.14) and consider the case $\Delta = -\omega_m$ and to perform a rotating wave approximation. Thus the equations of motion for the mean values of the cavity and mechanical operators are

$$\langle \delta\dot{a} \rangle = \left[i\omega_m - \frac{\kappa}{2} \right] \langle \delta a \rangle + iG\langle \delta b \rangle \tag{4.20}$$

$$\langle \dot{\delta b} \rangle = \left[-i\omega_m - \frac{\gamma_m}{2} \right] \langle \delta b \rangle + iG(\langle \delta a \rangle. \tag{4.21}$$

Assuming that $\kappa \gg \gamma_m$, the eigenvalues of this differential equation are

$$\omega_\pm = \omega_m - i\frac{\kappa}{4} \pm \sqrt{G^2 - \left(\frac{\kappa}{4}\right)^4}. \tag{4.22}$$

Therefore for $G > \frac{\kappa}{4}$ we get two resonant frequencies which are separated by the amount of $2G$. This regime is known as the strong coupling regime and has been reached in [44, 45].

4.4 Phonon cavity

We have seen how a microwave cavity can be used to manipulate the motion of a mechanical resonator. In Publication II we showed that a second oscillation mode of the same mechanical resonator can be used as a phonon cavity which operates similarly to the photon cavity and thus makes it possible to observe similar phenomena such as cooling via the phonon cavity [46]. In Section 3.1 we derive the nonlinear coupling between different modes of the mechanical resonator. As a reminder those coefficients are

$$
\begin{aligned}
[\Omega^2]^n_m &= \frac{\omega_0^2}{\omega_s^2}\langle\chi_n''|\chi_m''\rangle + [(\tau_0 + 2\langle u_0'|u_0'\rangle)\langle\chi_n'|\chi_m'\rangle + 4\langle\chi_n'|u_0'\rangle\langle u_0'|\chi_m'\rangle] \\
&- \frac{V_g^2}{2m\omega_s^2 d^2}\int_0^1 \frac{d^2C[1-u_0]}{du_1^2}\chi_n(z)\chi_m(z)dz. \qquad (4.23) \\
\mathcal{T}^n_{mo} &= 2\langle u_0'|\chi_o'\rangle\langle\chi_n'|\chi_m'\rangle \\
&- \frac{V_g^2}{12m\omega_s^2 d^2}\int_0^1 \frac{d^3C[1-u_0]}{du_1^3}\chi_n(z)\chi_m(z)\chi_o(z)dz. \qquad (4.24) \\
\mathcal{F}^{no}_{mp} &= \frac{1}{2}\langle\chi_n'|\chi_m'\rangle\langle\chi_o'|\chi_p'\rangle \\
&- \frac{V_g^2}{48m\omega_s^2 d^2}\int_0^1 \frac{d^3C[1-hu_0]}{du_1^3}\chi_n(z)\chi_m(z)\chi_o(z)\chi_p(z)dz. \qquad (4.25)
\end{aligned}
$$

Therefore, scaling the amplitude of deformation dx_n with the zero point motion $x_n^{zp} = \sqrt{\frac{\hbar}{2m\omega_m}}$ and writing the Hamiltonian in a basis which diagonalizes $[\Omega^2]^n_m$ we obtain

$$
H = \sum_n \omega_n a_n^\dagger a_n + \sum_{nmo} \mathbb{T}_{mno} X_n X_m X_o + \sum_{nmo} \mathbb{F}_{mnop} X_n X_m X_o X_p \qquad (4.26)
$$

with $X_n = a_n^\dagger + a_n$, $\omega_n = \omega_s[\Omega_d]^n_n$, $\mathbb{T}_{nmo} = \frac{m\omega_s}{d} x_n^{zp} x_m^{zp} x_o^{zp} (\mathcal{T}_d)^n_{mo}$ and $\mathbb{F}_{nmop} = \frac{m\omega_s^2}{d^2} x_n^{zp} x_m^{zp} x_o^{zp} x_p^{zp} (\mathcal{F}_d)^{no}_{mp}$. Here the subscript d denotes that the tensors have been written in the basis which diagonalizes $[\Omega^2]$. Let us now concentrate on the nonlinear coupling between two different modes. As a consequence of the static deformation u_0 we obtain a coupling of the form $\mathbb{T}^{nmm} x_n x_m^2$ which within the rotating frame approximation reduces to $T^{nmm} x_n a_m^\dagger a_m$ and corresponds to the radiation pressure coupling. Therefore it is possible to cool and heat the mechanical mode n using the mechanical mode m as a phonon cavity, analogously to the cooling/heating of a mechanical mode using a photon cavity. The difference with the phonon cavity resides in the presence of other nonlinear coefficients. To figure out their impact one can write the equation of motion of mode n and m using the input-output formalism [39]. Applying a coherent drive f_p to mode m oscillating at frequency $\omega_p = \omega_m + \Delta$ and a thermal drive a_n^{in} to mode n, the equations of motion are

$$
\begin{aligned}
\dot{a}_n &= -i\Big[\omega_n + 4F_n X_n^3 + 3T_n X_n^2 + 4F_{nnmm}\left(a_n^\dagger a + \frac{1}{2}\right) X_n \\
&\quad + 2T_{nmm}\left(a_m^\dagger a_m + \frac{1}{2}\right)\Big] - \frac{\gamma_n}{2} a_n + \sqrt{\gamma_n} a_n^{in} \qquad (4.27) \\
\dot{a}_m &= -i\Big[-\Delta + 12F_m a_m (a_m^\dagger a_m) \\
&\quad + 2(T_{nmm} X_n + F_{nnmm} X_n^2)\alpha_m\Big] - \frac{\gamma_n}{2} a_m + f_p. \qquad (4.28)
\end{aligned}
$$

Here we have written the equation of motion in a frame rotating with frequency ω_p and neglected fast oscillating terms. The nonlinear coeffi-

cients T_{nmo} and F_{nmop} are the sum of all the permutations of the indices n, m, o, p of $\mathbb{T}_{nmo}$ and $\mathbb{F}_{nmop}$, $T_n = T_{nnn}$. Similarly to Section 4.2, splitting the operators as the sum of a coherent α and thermal fluctuation parts δa, $a = \alpha + \delta a$ and solving δa_n for the thermal drive a_n^{in} we obtain a Lorentzian function which, in the fully sideband resolved limit $\omega_n \gg \gamma_m$, is peaked at $\omega_n + \omega_{\text{shift}}$ with

$$\frac{\omega_{\text{shift}}}{4|\alpha_m|^2} = \pm\frac{1}{2}T_{nmm}^2 + F_{nnmm} - 6T_n\frac{T_{nmm}}{\omega_n}, \tag{4.29}$$

its linewidth is $\gamma_n + \Gamma_{opt}$ with

$$\frac{\Gamma_{opt}}{4|\alpha_m|^2} = \pm\frac{T_{nmm}}{\gamma_m}, \tag{4.30}$$

where the upper sign refers to the red sideband ($\Delta = -\omega_n$) and the lower sign to the blue sideband ($\Delta = \omega_n$). In Eq. (4.29) the two first terms are the corrections from the radiation pressure coupling, the second term (F_{nnmm}) being a higher order correction and corresponding to a cross-Kerr coupling [47]. The difference from the usual optomechanical system shows up in the last term which is proportional to the self-nonlinearity T_n.

4.5 Enhancing the coupling

In Sec. 4.3, we discuss how by pumping more photons into the cavity one can reach the strong coupling regime. However, the physics there is still described by two linearly coupled harmonic oscillators. To be able to study the single-photon effect and to observe the optical frequency shift produced by the zero-point motion of the mechanical resonator, one needs to obtain a large coupling g. In Publication III we studied the effect of the nonlinearities coming from Josephson junctions when the latter are coupled to a cavity and a mechanical resonator. We showed that the radiation pressure coupling g can be enhanced by a large factor. To see how one can improve the coupling via the Josephson junctions let us consider a microwave cavity coupled to a single Cooper pair transistor. The latter consists of two Josephson junctions with small capacitances C_1 and C_2 and a gate capacitance $C_m(x)$ which depends on the amplitude x of the vibration of the mechanical resonator (see Fig. 4.4). The Lagrangian of the circuit is

$$\begin{aligned}\mathcal{L}_c = \frac{1}{2}C_0\dot{\phi}^2 + \frac{C_1}{2}\left(\dot{\phi}_I - \frac{\dot{\phi}}{2}\right)^2 + \frac{C_2}{2}\left(\dot{\phi}_I + \frac{\dot{\phi}}{2}\right)^2 + \frac{1}{2}C_m(x)(V_g - \dot{\phi}_I)^2 \\ - \frac{\phi^2}{2L} + E_{j1}\cos\left(\frac{\phi_I}{\phi_0} - \frac{1}{2}\frac{\phi}{\phi_0}\right) + E_{j2}\cos\left(\frac{\phi_I}{\phi_0} + \frac{1}{2}\frac{\phi}{\phi_0}\right),\end{aligned} \tag{4.31}$$

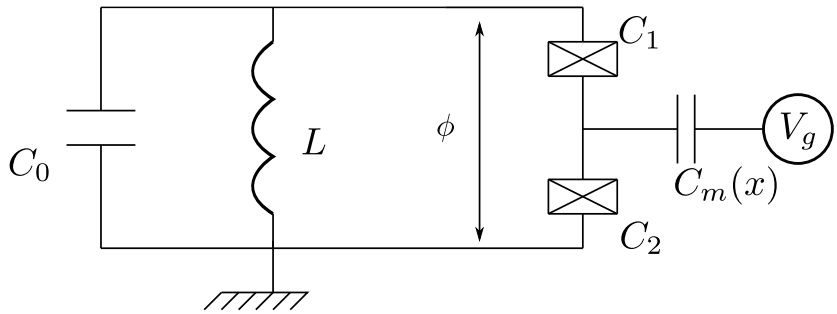

Figure 4.4. Optomechanical system studied here. The crossed boxes are the Josephson junctions and the mechanical resonator is taken into account via the capacitance $C_m(x)$.

where the two last terms are coming from the Josephson junctions and E_{j1} and E_{j2} are the Josephson energies associated to each Josephson junction and $\phi_0 = \frac{\hbar}{2e}$. From this Lagrangian the conjugate charges are

$$\begin{aligned} 2en &= \frac{\partial \mathcal{L}_c}{\partial \dot{\phi}} \\ &= \left(2C_0 + \frac{C_1+C_2}{2}\right)\frac{\dot{\phi}}{2} + (C_2 - C_1)\frac{\dot{\phi}_I}{2} \qquad (4.32) \\ 2en_I &= \frac{\partial \mathcal{L}_c}{\partial \dot{\phi}_I} \\ &= (C_m(x) + C_1 + C_2)\frac{\dot{\phi}_I}{2} + (C_2 - C_1)\frac{\dot{\phi}}{2} \qquad (4.33) \\ &\quad -C_m(x)V_g. \end{aligned}$$

Thus the Hamiltonian of the circuit is

$$\begin{aligned} \mathcal{H}_c = 4E_{C0}n^2 + 4Ec\left[n_I + \frac{C_m(x)V_g}{2e}\right]^2 + 4E_{cm}n\left[n_I + \frac{C_m(x)V_g}{2e}\right] - \frac{C_m(x)V_g^2}{2} \\ + \frac{\phi^2}{2L} - E_{j1}\cos\left(\frac{\phi_I}{\phi_0} - \frac{1}{2}\frac{\phi}{\phi_0}\right) - E_{j2}\cos\left(\frac{\phi_I}{\phi_0} + \frac{1}{2}\frac{\phi}{\phi_0}\right) \qquad (4.34) \end{aligned}$$

with

$$\begin{aligned} E_{C0} &= \frac{2(C_1 + C_2 + C_m(x))e^2}{4C1C2 + 4C_0[C_1 + C_2 + C_m(x)] + C_m(x)[C_1 + C_2])} \qquad (4.35) \\ E_C &= \frac{[2C_0 + \frac{C_1+C_2}{2}]e^2}{4C1C2 + 4C_0[C_1 + C_2 + C_m(x)] + C_m(x)[C_1 + C_2])} \qquad (4.36) \\ E_{Cm} &= \frac{2(C_1 - C_2)e^2}{4C1C2 + 4C_0[C_1 + C_2 + C_m(x)] + C_m(x)[C_1 + C_2])} \qquad (4.37) \end{aligned}$$

In the limit $E_c \gg E_{j1}, E_{j2}$ a fair approximation for the single Cooper pair transistor is obtain by projecting the Hamiltonian to the two charge states closest to $C_m(0)V_g$. Making the substitution [48],

$$\cos(\phi_I) \to \frac{1}{2}\sigma_x, \tag{4.38}$$

$$\sin(\phi_I) \to \frac{1}{2}\sigma_y, \tag{4.39}$$

$$\left[n_I + \frac{C_m(x)V_g}{2e}\right]^2 \to \frac{1}{2}\left(1 + \frac{C_m(x)V_g}{e}\right)\sigma_z. \tag{4.40}$$

To simplify our analysis we consider the case of symmetric junctions with $C_1 = C_2$ and $E_{j1} = E_{j2} = E_j$, thus the Hamiltonian for the circuit reduces to

$$\mathcal{H}_c = 4E_{C0}n^2 + \frac{\phi^2}{2L} + 2E_c\left[1 + \frac{C_m(x)V_g}{e}\right]\sigma_z - E_j\cos\left[\frac{\phi}{2}\right]\sigma_x. \tag{4.41}$$

Therefore in the limit where $C_0 \gg C_m, C_1, C_2$and expanding the $\cos$ term around $\phi = 0$, including the mechanical resonator the total Hamiltonian is

$$\mathcal{H} = \hbar\omega_c a^\dagger a + \hbar\omega_m b^\dagger b + 2E_c\left[1 + \frac{C_m(x)V_g}{e}\right]\sigma_z - E_j(1 + \frac{\phi^2}{8})\sigma_x. \tag{4.42}$$

Here $\omega_c = \frac{1}{\sqrt{LC_0}}$ is the frequency of the cavity, ω_m the frequency of the mechanical vibration where we defined

$$\phi = \sqrt{\frac{\hbar}{2C_0\omega_c}}(a^\dagger + a), \tag{4.43}$$

$$n = i\sqrt{\frac{C_0\hbar\omega_c}{8e^2}}(a^\dagger - a). \tag{4.44}$$

Assuming that the energy of the qubit is larger than the energy of the mechanical resonator $\hbar\omega_m$ and the cavity $\hbar\omega_c$ we can diagonalize the qubit part treating the oscillator coordinate as a scalar and therefore considering the case where the qubit is in its ground state the Hamiltonian is

$$\mathcal{H} = \hbar\omega_c a^\dagger a + \hbar\omega_m b^\dagger b - g_m\frac{B_z}{|B|}x - \frac{B_x^2}{8|B|}\left(\frac{\phi}{\phi_0}\right)^2 + g_m\frac{B_z B_x^2}{8|B|^3}x\left(\frac{\phi}{\phi_0}\right)^2. \tag{4.45}$$

Here $B_x = -E_j$, $B_z = 2E_c\left(1 + \frac{V_g C_m(0)}{e}\right)$ and $g_m = 2E_C C_m'(0)V_g x_{zp}$. The first two terms correspond to free oscillators. The third term is a qubit induced drive of the mechanical resonator, the fourth term is a cavity Stark shift and the final term corresponds to a radiation-pressure coupling between the cavity and the mechanical resonator. Because the radiation pressure coupling is proportional to $C_m(0)V_g$, it is possible to amplify the coupling with the gate voltage V_g. It offers the possibility of observing higher order nonlinear effects especially the cross-Kerr effect which we discuss in the next section.

4.6 Cross-Kerr nonlinearity

We show in Sec. 4.5 that the radiation pressure coupling can be improved leading to additional nonlinear interaction namely the cross-Kerr coupling g_{ck}. This nonlinear effect couples the number of photons in the cavity to the number of phonons in the mechanical resonator. This effect has also been observed in setups where the mechanical resonator was placed in the middle of an optical cavity [49, 50]. There the relative value of the cross-Kerr coupling g_{ck} with respect to the radiation pressure coupling g is a function of the position of the resonator while in our setup it on the value of the gate charge to the superconducting island. The effect of this coupling and how the results deviate from the radiation pressure coupling are investigated in Publication IV. In order to understand the idea behind Publication IV let us make the same thought process which has lead to the analysis made in Publication IV. The Hamiltonian of a cavity with frequency ω_c and a mechanical resonator with frequency ω_m couple to each other via the radiation pressure coupling g and the cross-Kerr coupling g_{ck} can be written as

$$H = \omega_c a^\dagger a + \omega_m b^\dagger b - g a^\dagger a (b^\dagger + b) - g_{ck} a^\dagger a b^\dagger b, \tag{4.46}$$

where a and b are the operators associated to the cavity and the mechanical resonator respectively. Using the input-output formalism [39] the equation of motions are

$$\dot{a}(t) = -i(-\Delta)a + ig\, a(b^\dagger + b) + ig_{ck} a b^\dagger b - \frac{\kappa}{2}a - \sqrt{\kappa}a_{in} \tag{4.47}$$

$$\dot{b}(t) = -i\omega_m b + ig\, a^\dagger a + ig_{ck}\, a^\dagger a\, b - \frac{\gamma}{2}b - \sqrt{\gamma}b_{in}. \tag{4.48}$$

and their complex conjugate. Here we have considered that the cavity field is driven with a coherent field of strength f_p oscillating at the frequency $\omega_p = \omega_c + \Delta$. In addition we have written the cavity operator a in a frame rotating with frequency ω_p and neglected the fast oscillating terms. We define κ to be the damping rate of the cavity and γ the damping rate of the mechanical mode. To solve the dynamic of the cavity and the resonator we make a perturbation expansion. We assume that the radiation-pressure coupling $g \propto \mathcal{O}(\epsilon)$ and the cross-Kerr coupling $g_{ck} \propto \mathcal{O}(\epsilon^2)$ with $\epsilon \ll 1$. Moreover, we assume that the solutions for the cavity and the resonator are the sum of the unperturbed harmonic oscillator and the sum of the small perturbation coming from the g and g_{ck},

$$a = a_0 + \epsilon a_1 + \epsilon^2 a_2, \tag{4.49}$$

$$b = b_0 + \epsilon b_1 + \epsilon^2 b_2. \tag{4.50}$$

We also use the Fourier transform definition

$$a(\omega) = \int e^{-i\omega t} a(t) dt, \tag{4.51}$$

$$a^\dagger(\omega) = \int e^{-i\omega t} a^\dagger(t) dt, \tag{4.52}$$

$$b(\omega) = \int e^{-i\omega t} b(t) dt, \tag{4.53}$$

$$b^\dagger(\omega) = \int e^{-i\omega t} b^\dagger(t) dt. \tag{4.54}$$

This Fourier transformation implies that $a^\dagger(\omega) = [a(-\omega)]^\dagger$ and the same for $b^\dagger(\omega)$.

The $\mathcal{O}(\epsilon^0)$ corresponds to the case where the cavity and the resonator are not coupled. The solutions are a driven harmonic oscillator with driving a_{in} for the cavity and b_{in} for the resonator.

$$a_0(\omega) = \frac{\sqrt{\kappa}}{\frac{\kappa}{2} - i(\omega + \Delta)} a_0^{in}(\omega) \equiv \chi_{-\Delta}(\omega) a_0^{in}(\omega) \tag{4.55}$$

$$a_0^\dagger(\omega) = \frac{\sqrt{\kappa}}{\frac{\kappa}{2} - i(\omega - \Delta)} a_0^{in\dagger}(\omega) \equiv \chi_{\Delta}(\omega) a_0^{in\dagger}(\omega) \tag{4.56}$$

$$b_0(\omega) = \frac{\sqrt{\gamma}}{\frac{\gamma}{2} - i(\omega - \omega_m)} b_0^{in}(\omega) \equiv \chi_{\omega_m}(\omega) b_0^{in}(\omega) \tag{4.57}$$

$$b_0^\dagger(\omega) = \frac{\sqrt{\gamma}}{\frac{\gamma}{2} - i(\omega + \omega_m)} b_0^{in\dagger}(\omega) \equiv \chi_{-\omega_m}(\omega) b_0^{in\dagger}(\omega). \tag{4.58}$$

Below, we assume that the cavity input field $a_0^{in}(\omega) = f_p \delta(\omega)$ and assume that the mechanical resonator is driven by thermal noise which satisfies $\langle b_{in} \rangle = 0$ and $\langle b_{in}^\dagger(\omega') b_{in}(\omega) \rangle = n^{th} \delta(\omega + \omega')$ with n^{th} being the number of thermal phonons in the mechanical resonator.

With $\mathcal{O}(\epsilon)$ we include the radiation pressure effect. The correction to the cavity added by this coupling is

$$\begin{aligned} a_1 &= i\frac{g}{\sqrt{\kappa}} \chi_{-\Delta}(\omega) f_p \chi_{-\Delta}(0) [b_0^\dagger(\omega) + b_0(\omega)] \\ a_1^\dagger &= i\frac{g}{\sqrt{\kappa}} \chi_{\Delta}(\omega) f_p^* \chi_{\Delta}(0) [b_0^\dagger(\omega) + b_0(\omega)] \end{aligned}$$

As expected from Sec. 4.1, the correction to the cavity is proportional to the thermal motion of the mechanical resonator. The power spectrum is

$$\langle a_1^\dagger(-\omega) a_1(\omega) \rangle = \langle a_1^\dagger(-\omega) a_1(\omega) \rangle_{\text{red}} + \langle a_1^\dagger(-\omega) a_1(\omega) \rangle_{\text{blue}} \tag{4.59}$$

with

$$\begin{aligned} \langle a_1^\dagger(-\omega) a_1(\omega) \rangle_{\text{blue}} &= g^2 |\alpha|^2 |\chi_{-\Delta}(\omega)|^2 |\chi_{\omega_m}(\omega)|^2 \langle b_{in}^\dagger b_{in} \rangle, \\ \langle a_1^\dagger(-\omega) a_1(\omega) \rangle_{\text{red}} &= g^2 |\alpha|^2 |\chi_{-\Delta}(\omega)|^2 |\chi_{\omega_m}(-\omega)|^2 \langle b_{in} b_{in}^\dagger \rangle. \end{aligned}$$

and $|\alpha|^2 = \frac{|f_p|^2}{\kappa^2/4 + \Delta^2}$ is the number of photons pumped into the cavity. The correction from the radiation pressure gives an additional resonance peak

at $\omega = \omega_m$ and $\omega = -\omega_m$. These two resonances correspond to the blue sideband and the red sideband respectively.

With $\mathcal{O}(\epsilon^2)$ we include the cross-Kerr effect. The correction induced by the cross-Kerr coupling is $2\mathrm{Re}(\langle a_0^\dagger(-\omega)a_2^{ck}(\omega)\rangle)$ with

$$\begin{aligned} a_2^{ck}(\omega) &= i\frac{g_{ck}}{\sqrt{\kappa}} f_p \chi_{-\Delta}(\omega)\chi_{-\Delta}(0)\delta(\omega)\int \chi_{-\omega_m}(\omega-\Omega)\chi_{\omega_m}(\Omega)\frac{d\Omega}{2\pi}, \\ &= i\frac{g_{ck}}{\sqrt{\kappa}} f_p \chi_{-\Delta}(\omega)\chi_{-\Delta}(0)\delta(\omega)\frac{\gamma}{\gamma - i\omega}. \end{aligned} \tag{4.60}$$

We obtain

$$2\mathrm{Re}(\langle a_0^\dagger(-\omega)a_2^{ck}(\omega)\rangle) = 2\mathcal{G}_{ck}\mathrm{Re}\left(i\chi_{-\Delta}(0)\frac{\gamma}{\gamma - i\omega}\right)\langle a_0^\dagger(-\omega)a_0(\omega)\rangle, \tag{4.61}$$

Therefore the cross-Kerr effect gives a correction to the main resonance which is proportional to the number of thermal phonons n^{th} in the resonator. With Eq. (4.61) the main resonance becomes

$$\langle a_0^\dagger(-\omega)a_0(\omega)\rangle\left[1 + 2\frac{g_{ck}}{\sqrt{\kappa}}n^{th}\mathrm{Re}\left(i\chi_{-\Delta}(0)\frac{\gamma}{\gamma - i\omega}\right)\right] \tag{4.62}$$

Equation (4.62) corresponds to the beginning of the Taylor expansion of

$$\frac{|f_p|^2\kappa}{\kappa^2/4 + \Delta(\Delta + 2g_{ck}n_{\omega_n})}. \tag{4.63}$$

Therefore, we have a frequency shift which is proportional to the number of thermal phonons in the mechanical resonator.

The next order of the perturbation giving corrections to the power spectrum is $\mathcal{O}(\epsilon^4)$. We only focus on terms which give correction to the sidebands. Those terms are $\mathrm{Re}(\langle a_1^\dagger(-\omega)a_3^{ck}(\omega)\rangle)$ and $\mathrm{Re}(\langle a_1^\dagger(-\omega)a_3^{rp}(\omega)\rangle)$ with

$$\begin{aligned} a_3^{ck}(\omega) &= i\frac{\chi_{-\Delta}(\omega)}{\sqrt{\kappa}}\left(g_{ck}\int b_0^\dagger(\omega-\Omega-\Omega')b_0(\Omega')a_1(\Omega)d\Omega d\Omega'\right), \\ a_3^{rp}(\omega) &= -i\frac{g^2}{\sqrt{\kappa}}\chi_{-\Delta}(\omega)\Bigg[\int a_2^{rp}(\omega-\Omega)(b_0^\dagger(\Omega)+b_0(\Omega))\frac{d\Omega}{2\pi} \\ &\quad + \int a_0^{rp}(\omega-\Omega)(b_2^{rp^\dagger}(\Omega)+b_2^{rp}(\Omega))\frac{d\Omega}{2\pi} \\ &\quad + \int a_1(\omega-\Omega)(b_1^\dagger(\Omega)+b_1(\Omega))\frac{d\Omega}{2\pi}\Bigg], \\ a_2^{rp}(\omega) &= i\frac{g}{\sqrt{\kappa}}\chi_{-\Delta}(\omega)\int (b_0^\dagger(\omega-\Omega)+b_0(\omega-\Omega))a_1(\Omega)\frac{d\Omega}{2\pi} \\ b_2^{rp}(\omega) &= i\frac{g}{\sqrt{\gamma}}\chi_{\omega_m}\left[\chi_\Delta(0)f_p^* a_1(\omega) + \chi_{-\Delta}(0)f_p a_1^\dagger(\omega)\right] \end{aligned}$$

In the resolved sideband regime ($\kappa \ll \omega_m$) for $\Delta = -\omega_m$ and $\omega \sim \omega_m$ the expression for the red sideband becomes

$$\langle a_1^\dagger(-\omega)a_1(\omega)\rangle_{\mathrm{red}}\left[1 + 2\mathrm{Re}\left(i\chi_{-\Delta}(\omega)\left\{i\frac{g^2|\alpha|^2}{\sqrt{\kappa\gamma}}\chi_{-\omega_m}(\omega) - \frac{g_{ck}n^{th}}{\sqrt{\kappa}}\right\}\right)\right], \tag{4.64}$$

and for $\Delta = \omega_m$ and $\omega \sim -\omega_m$ the expression for the blue sideband becomes

$$\langle a_1^\dagger(-\omega)a_1(\omega)\rangle_{\text{blue}}\left[1 - 2\text{Re}\left(i\chi_{-\Delta}(\omega)\left\{i\frac{g^2|\alpha|^2}{\sqrt{\kappa\gamma}}\chi_{-\omega_m}(\omega) + \frac{g_{ck}n^{th}}{\sqrt{\kappa}}\right\}\right)\right], \quad (4.65)$$

Equations (4.64) and (4.65) correspond to the beginning of the Taylor expansions for the red side of

$$\frac{G^2\gamma n_{\omega_m}}{|\chi_{-\omega_m}|^2[\kappa^2/4 + (\omega+\Delta)(\omega+\Delta+2g_{ck}n^{th})] + 2G^2\kappa\left[(\omega+\Delta)(\omega+\omega_m) - \frac{\gamma\kappa}{4}\right]} \quad (4.66)$$

and for the blue side

$$\frac{G^2\gamma(n_{\omega_m}+1)}{|\chi_{\omega_m}|^2[\kappa^2/4 + (\omega+\Delta)(\omega+\Delta+2g_{ck}n^{th})] + 2G^2\left[(\omega+\Delta)(\omega-\omega_m) - \frac{\gamma\kappa}{4}\right]}, \quad (4.67)$$

with $G = g|\alpha|$. Once again the effect of the cross-Kerr effect it to shift the sideband peak to a quantity proportional to the thermal occupation of the mechanical resonator. Moreover we recognize that the denominator in Eq. (4.63) is the beginning of $\kappa^2/4 + (\Delta + g_{ck}n^{th})^2$ and that in Eqs (4.66) and (4.67), $\kappa^2/4 + (\omega+\Delta)(\omega+\Delta+2g_{ck}n^{th})$ is the beginning of $\kappa^2/4 + (\omega+\Delta+g_{ck}n^{th})^2$. Higher order corrections in the perturbation theory should complete the squares. However it would require to go up to $\mathcal{O}(\epsilon^4)$ to see this correction on the main resonance peak and to go up to $\mathcal{O}(\epsilon^6)$ to see the correction on the sideband peak. Therefore in Publication IV we choose to treat the problem using a mean field approach. Using a mean-field approach to treat the radiation pressure coupling and the cross-Kerr coupling, one obtains for the first one

$$ga^\dagger a(b^\dagger + b) = g\Big[(\langle a^\dagger\rangle a + \langle a\rangle a^\dagger - \langle a^\dagger a\rangle)(b^\dagger + b) + (a^\dagger a - \langle a\rangle a^\dagger - \langle a^\dagger\rangle a)\langle b^\dagger + b\rangle\Big]. \quad (4.68)$$

This decomposition allows us to find the usual results of the radiation pressure coupling discussed in Sec. 4.1. The first line of Eq. (4.68) describes exchange processes between the cavity and the resonator and the second is a frequency shift of the cavity. For the cross-Kerr coupling we approximate

$$g_{ck}a^\dagger a b^\dagger b = g_{ck}\Big[\langle a^\dagger a\rangle b^\dagger b + \langle b^\dagger b\rangle a^\dagger a + \langle b^\dagger a\rangle b a^\dagger + \langle b a^\dagger\rangle b^\dagger a + \langle ba\rangle b^\dagger a^\dagger + \langle b^\dagger a^\dagger\rangle ba\Big]. \quad (4.69)$$

The first line of Eq. (4.69) corresponds to a coupling between the number of photons in the cavity and a mean field created by the number of

phonons in the resonator and vice versa. The other terms describe exchange processes between the resonator and the cavity. We can now proceed as in Sec. 4.2. Using the input output formalism and after splitting the operators into a sum of a coherent and fluctuation part we obtain for the fluctuations

$$\left[\frac{\kappa}{2} - i(\omega + \tilde{\Delta})\right] \delta a = i\mathcal{G}\alpha\delta b^\dagger + i\mathcal{G}^*\alpha\delta b \tag{4.70}$$

$$\left[\frac{\gamma}{2} - i(\omega - \tilde{\omega}_m)\right] \delta b = i\mathcal{G}\alpha^*\delta a + i\mathcal{G}\alpha\delta a^\dagger + \sqrt{\gamma}b_{in}. \tag{4.71}$$

These equations are similar to the onse derived in Sec. 4.2. The difference resides in the fact that the radiation pressure coupling is modified by the cross-Kerr coupling and one has $\mathcal{G} = g + g_{ck}\langle b\rangle$. Moreover, the detuning and frequency are now $\tilde{\Delta} = \Delta + g_{ck}\langle b^\dagger b\rangle$ and $\tilde{\omega}_m = \omega_m - g_{ck}\langle a^\dagger a\rangle$, where $\langle a^\dagger a\rangle = |\alpha|^2 + \langle \delta a^\dagger \delta a\rangle$ ($\langle b^\dagger b\rangle = |\beta|^2 + \langle \delta b^\dagger \delta b\rangle$) is the mean field of the number of photons (phonons) in the cavity (mechanical resonator) and consists of a sum of a coherent and fluctuation part. These mean fields need to be solved self-consistently using

$$\alpha = \frac{\sqrt{\kappa} f_p}{\frac{\kappa}{2} - i[\Delta - g_{ck}\langle b^\dagger b\rangle - (G^*\beta + G\beta^*)]}, \tag{4.72}$$

$$\beta = \frac{i(2G - g)|\alpha|^2 - ig\langle \delta a^\dagger \delta a\rangle}{\gamma/2 + i(\omega_m - g_{ck}\langle a^\dagger a\rangle)}. \tag{4.73}$$

for the coherent part and for the fluctuation part we get [40]

$$\langle \delta b^\dagger \delta b\rangle = \frac{\gamma n^{th} + \Gamma_{opt} n_{m_0}}{\gamma + \Gamma_{\rm opt}}, \tag{4.74}$$

$$\langle \delta a^\dagger \delta a\rangle = G^2|\alpha|^2\langle \delta b^\dagger \delta b\rangle \left(\frac{1}{\frac{\kappa^2}{4} + (\tilde{\omega}_m + \tilde{\Delta})^2} + \frac{1}{\frac{\kappa^2}{4} + (\tilde{\omega}_m - \tilde{\Delta})^2}\right). \tag{4.75}$$

The validity of the mean field in Eqs. (4.68) and (4.69) is given by the condition $\langle \delta a^\dagger \delta a\rangle \ll |\alpha|^2$ which reduces to the following condition

$$\langle \delta b^\dagger \delta b\rangle \ll G^{-2}\left(\frac{1}{\frac{\kappa^2}{4} + (\tilde{\omega}_m + \tilde{\Delta})^2} + \frac{1}{\frac{\kappa^2}{4} + (\tilde{\omega}_m - \tilde{\Delta})^2}\right)^{-1}. \tag{4.76}$$

The effects on the cooling and heating processes can be studied by substituting in (4.17) ω_m with $\tilde{\omega}_m$, Δ with $\tilde{\Delta}$ and G with $\mathcal{G}\alpha$. We obtain

$$\Gamma_{\rm opt} = \mathcal{G}^2|\alpha|^2\kappa\left[\frac{1}{\frac{\kappa^2}{4} + (\tilde{\omega}_m + \tilde{\Delta})^2} - \frac{1}{\frac{\kappa^2}{4} + (\tilde{\omega}_m - \Delta)^2}\right]. \tag{4.77}$$

The effect of the cross-Kerr coupling depends on the detuning. In the case where $\tilde{\Delta} = \mp\tilde{\omega}_m$ the result is identical to the one obtained usually in optomechanics in absence of the cross-Kerr. Namely we obtain

$$\Gamma_{\rm opt} = \pm\frac{4\mathcal{G}|\alpha|^2}{\kappa}, \tag{4.78}$$

where the upper sign refers to the red sideband ($\tilde{\Delta} = -\tilde{\omega}_m$) and the lower sign to the blue sideband ($\tilde{\Delta} = -\tilde{\omega}_m$) . To see the effects of the cross-Kerr one has to set $\Delta = \mp\omega_m$ which translates to $\tilde{\Delta} = \mp\omega_m + g_{ck}\langle b^\dagger b\rangle$. This case is more realistic since in the experiments the parameter one has access to directly is the detuning Δ and not $\tilde{\Delta}$ In this case we get

$$\Gamma_{\rm opt} = \pm\frac{\mathcal{G}|\alpha|^2\kappa}{g_{ck}^2(\langle b^\dagger b\rangle - \langle a^\dagger a\rangle)^2 + \frac{\kappa^2}{4}} \tag{4.79}$$

The main effect of the cross-Kerr coupling is for the red sideband and the blue sideband to change the behavior of the optical damping from a linear to a nonmonotonous function of the number of photons pumped into the cavity. As discussed in Publication IV, for the red sideband the optical damping shows a maximum at $|\alpha|^2 = \kappa/(2g_{ck})$. As a consequence one can cool the mechanical resonator to $\langle \delta b^\dagger \delta b\rangle = \gamma n^{th}/(\gamma + \mathcal{G}/g_{ck})$. This estimate is valid for $n^{th} \ll \kappa/(2g_{ck})[1 + g^2/\gamma g_{ck}]$. For the blue sideband the main effect of the cross-Kerr coupling is to limit the instability to a finite number of photons $\langle \delta b^\dagger \delta b\rangle \approx \sqrt{\kappa/\gamma}\mathcal{G}|\alpha|^2/g_{ck} + |\alpha|^2$. When $g_{ck} \gg \kappa/(4n^{th})$ the instability is completely prevented.

5. Outlook

In the previous chapters we discuss the background of the publications present in this dissertation on nanomechanical and optomechanical systems. We have shown how nonlinearities can be used to observe macroscopic quantum tunneling and how they can be used to cool a mode of a resonator to its ground state. Although the field of nanoelectromechanical systems (NEMS) is relatively new, applications are already conceivable. Similar to their precursor, the microelectromechanical systems, NEMS show promising possibility for atomic force microscope (AFM) [51, 52, 53]. The advances of mass sensing using NEMS have increased significantly and it has been demonstrated that spatial distributions of mass within a chemical subtance can be imaged in real time and at a molecular scale [54]. Also for sensing applications, cavity optomechanics bring several innovations and possibilities such as magnetometry or accelerometry [55, 56]. Nanomechanical systems also offer a framework to study nonlinear dynamics which might prove useful for future nanotechnological applications [57]. Among the reasons which have increased the importance of cavity optomechanics, is the possibility to use the latter as a light/matter interface and converting microwave to optical frequencies and vice versa. For example in [58] the interaction between a microwave cavity, a qubit and vibration mode of a resonator has been investigated. Another interesting direction is the effort to make the bare radiation pressure coupling of the order of the linewidth of the cavity. Within this regime, the effect of a single photon on the resonator is observable and one should be able to observe a optical frequency shift produced by the zero point motion of the mechanical resonator. Last but not the least, NEMS also offer the possibility to test the foundations of quantum mechanics [59]. Right now there is no indication that quantum mechanics should break down for macroscopic system (made of billions of atoms). However it seems that

quantum phenomena do not occur at this large scale. There is some decoherence mechanisms which prevent macroscopic system to behave in a quantum way. NEMS may offer a framework to investigate the border between the classical world and the quantum world.

Bibliography

[1] C. A. Coulomb, "Premier mémoire sur l'électricité et le magnétisme," *Histoire de l'Académie Royale des Sciences. Imprimerie Royale.*, p. 569, 1785.

[2] G. T. Gillies, "The newtonian gravitational constant: an index of measurements," *Metrologia*, vol. 24, no. S, p. 1, 1987.

[3] E. Gavartin, P. Verlot, and T. Kippenberg, "A hybrid on-chip optomechanical transducer for ultrasensitive force measurements," *Nature Nanotechnology*, vol. 7, no. 8, pp. 509–514, 2012.

[4] K. Jensen, K. Kim, and A. Zettl, "An atomic-resolution nanomechanical mass sensor," *Nature Nanotechnology*, vol. 3, no. 9, pp. 533–537, 2008.

[5] K. Ekinci, X. Huang, and M. Roukes, "Ultrasensitive nanoelectromechanical mass detection," *Applied Physics Letters*, vol. 84, no. 22, pp. 4469–4471, 2004.

[6] J. Chaste, A. Eichler, J. Moser, G. Ceballos, R. Rurali, and A. Bachtold, "A nanomechanical mass sensor with yoctogram resolution," *Nature Nanotechnology*, vol. 7, no. 5, pp. 301–304, 2012.

[7] M. Bordag, U. Mohideen, and V. Mostepanenko, "New developments in the casimir effect," *Physics Reports*, vol. 353, no. 1–3, pp. 1 – 205, 2001.

[8] A. D. O'Connell, M. Hofheinz, M. Ansmann, R. C. Bialczak, M. Lenander, E. Lucero, M. Neeley, D. Sank, H. Wang, M. Weides, *et al.*, "Quantum ground state and single-phonon control of a mechanical resonator," *Nature*, vol. 464, no. 7289, pp. 697–703, 2010.

[9] J. Teufel, T. Donner, D. Li, J. Harlow, M. Allman, K. Cicak, A. Sirois, J. D. Whittaker, K. Lehnert, and R. W. Simmonds, "Sideband cooling of micromechanical motion to the quantum ground state," *Nature*, vol. 475, no. 7356, pp. 359–363, 2011.

[10] W. Marshall, C. Simon, R. Penrose, and D. Bouwmeester, "Towards quantum superpositions of a mirror," *Physical Review Letters*, vol. 91, p. 130401, 2003.

[11] A. A. Clerk, F. Marquardt, and K. Jacobs, "Back-action evasion and squeezing of a mechanical resonator using a cavity detector," *New Journal of Physics*, vol. 10, no. 9, p. 095010, 2008.

[12] D. Vitali, S. Gigan, A. Ferreira, H. Böhm, P. Tombesi, A. Guerreiro, V. Vedral, A. Zeilinger, and M. Aspelmeyer, "Optomechanical entanglement between a movable mirror and a cavity field," *Physical Review Letters*, vol. 98, p. 030405, 2007.

[13] C. Fabre, M. Pinard, S. Bourzeix, A. Heidmann, E. Giacobino, and S. Reynaud, "Quantum-noise reduction using a cavity with a movable mirror," *Physical Review A*, vol. 49, no. 2, p. 1337, 1994.

[14] S. Mancini, V. Giovannetti, D. Vitali, and P. Tombesi, "Entangling macroscopic oscillators exploiting radiation pressure," *Physical Review Letters*, vol. 88, no. 12, p. 120401, 2002.

[15] L. Landau and E. Lifchitz, "Theory of elasticity," 1990.

[16] T. T. Heikkilä, *The Physics of Nanoelectronics: Transport and Fluctuation Phenomena at Low Temperatures*, vol. 21. Oxford University Press, 2013.

[17] A. N. Cleland, *Foundations of nanomechanics: from solid-state theory to device applications*. Springer Science & Business Media, 2002.

[18] C. A. Fletcher, *Computational galerkin methods*. Springer, 1984.

[19] X. Song, M. Oksanen, M. A. Sillanpää, H. Craighead, J. Parpia, and P. J. Hakonen, "Stamp transferred suspended graphene mechanical resonators for radio frequency electrical readout," *Nano Letters*, vol. 12, no. 1, pp. 198–202, 2011.

[20] C. Chen, S. Rosenblatt, K. I. Bolotin, W. Kalb, P. Kim, I. Kymissis, H. L. Stormer, T. F. Heinz, and J. Hone, "Performance of monolayer graphene nanomechanical resonators with electrical readout," *Nature Nanotechnology*, vol. 4, no. 12, pp. 861–867, 2009.

[21] V. Sazonova, Y. Yaish, H. Üstünel, D. Roundy, T. A. Arias, and P. L. McEuen, "A tunable carbon nanotube electromechanical oscillator," *Nature*, vol. 431, no. 7006, pp. 284–287, 2004.

[22] I. Kozinsky, H. C. Postma, I. Bargatin, and M. Roukes, "Tuning nonlinearity, dynamic range, and frequency of nanomechanical resonators," *Applied Physics Letters*, vol. 88, no. 25, p. 253101, 2006.

[23] J. Atalaya, J. M. Kinaret, and A. Isacsson, "Nanomechanical mass measurement using nonlinear response of a graphene membrane," *Europhysics Letters*, vol. 91, no. 4, p. 48001, 2010.

[24] W. Zhang, R. Baskaran, and K. L. Turner, "Effect of cubic nonlinearity on auto-parametrically amplified resonant mems mass sensor," *Sensors and Actuators A: Physical*, vol. 102, no. 1, pp. 139–150, 2002.

[25] R. Lifshitz and M. Cross, "Nonlinear dynamics of nanomechanical and micromechanical resonators," *Review of nonlinear dynamics and complexity*, vol. 1, pp. 1–52, 2008.

[26] A. H. Nayfeh and D. T. Mook, *Nonlinear oscillations*. John Wiley & Sons, 2008.

[27] H. Westra, M. Poot, H. Van der Zant, and W. Venstra, "Nonlinear modal interactions in clamped-clamped mechanical resonators," *Physical Review Letters*, vol. 105, no. 11, p. 117205, 2010.

[28] K. Lulla, R. Cousins, A. Venkatesan, M. Patton, A. Armour, C. Mellor, and J. Owers-Bradley, "Nonlinear modal coupling in a high-stress doubly-clamped nanomechanical resonator," *New Journal of Physics*, vol. 14, no. 11, p. 113040, 2012.

[29] S. Sapmaz, Y. M. Blanter, L. Gurevich, and H. S. J. van der Zant, "Carbon nanotubes as nanoelectromechanical systems," *Physical Review B*, vol. 67, p. 235414, Jun 2003.

[30] V. Kaajakari *et al.*, *Practical MEMS: Design of microsystems, accelerometers, gyroscopes, RF MEMS, optical MEMS, and microfluidic systems*. 2009.

[31] U. Weiss, *Quantum dissipative systems*, vol. 10. World Scientific, 1999.

[32] T. J. Kippenberg and K. J. Vahala, "Cavity optomechanics: back-action at the mesoscale," *Science*, vol. 321, no. 5893, pp. 1172–1176, 2008.

[33] J. Chan, T. M. Alegre, A. H. Safavi-Naeini, J. T. Hill, A. Krause, S. Gröblacher, M. Aspelmeyer, and O. Painter, "Laser cooling of a nanomechanical oscillator into its quantum ground state," *Nature*, vol. 478, no. 7367, pp. 89–92, 2011.

[34] I. Favero and K. Karrai, "Optomechanics of deformable optical cavities," *Nature Photonics*, vol. 3, no. 4, pp. 201–205, 2009.

[35] C. H. Metzger and K. Karrai, "Cavity cooling of a microlever," *Nature*, vol. 432, no. 7020, pp. 1002–1005, 2004.

[36] E. F. Nichols and G. Hull, "A preliminary communication on the pressure of heat and light radiation," *Physical Review (Series I)*, vol. 13, no. 5, p. 307, 1901.

[37] M. Aspelmeyer, T. J. Kippenberg, and F. Marquardt, "Cavity optomechanics," *Reviews of Modern Physics*, vol. 86, no. 4, p. 1391, 2014.

[38] F. Massel, T. Heikkilä, J.-M. Pirkkalainen, S. Cho, H. Saloniemi, P. Hakonen, and M. Sillanpää, "Microwave amplification with nanomechanical resonators," *Nature*, vol. 480, no. 7377, pp. 351–354, 2011.

[39] C. W. Gardiner and M. J. Collett, "Input and output in damped quantum systems: Quantum stochastic differential equations and the master equation," *Physical Review A*, vol. 31, pp. 3761–3774, Jun 1985.

[40] F. Marquardt, J. P. Chen, A. A. Clerk, and S. M. Girvin, "Quantum theory of cavity-assisted sideband cooling of mechanical motion," *Physical Review Letters*, vol. 99, p. 093902, Aug 2007.

[41] J. D. Teufel, J. W. Harlow, C. A. Regal, and K. W. Lehnert, "Dynamical backaction of microwave fields on a nanomechanical oscillator," *Physical Review Letters*, vol. 101, p. 197203, 2008.

[42] A. Schliesser, P. Del'Haye, N. Nooshi, K. J. Vahala, and T. J. Kippenberg, "Radiation pressure cooling of a micromechanical oscillator using dynamical backaction," *Physical Review Letters*, vol. 97, p. 243905, 2006.

[43] T. Kippenberg, H. Rokhsari, T. Carmon, A. Scherer, and K. Vahala, "Analysis of radiation-pressure induced mechanical oscillation of an optical microcavity," *Physical Review Letters*, vol. 95, no. 3, p. 033901, 2005.

[44] S. Gröblacher, K. Hammerer, M. R. Vanner, and M. Aspelmeyer, "Observation of strong coupling between a micromechanical resonator and an optical cavity field," *Nature*, vol. 460, no. 7256, pp. 724–727, 2009.

[45] J. D. Teufel, D. Li, M. Allman, K. Cicak, A. Sirois, J. Whittaker, and R. Simmonds, "Circuit cavity electromechanics in the strong-coupling regime," *Nature*, vol. 471, no. 7337, pp. 204–208, 2011.

[46] I. Mahboob, K. Nishiguchi, H. Okamoto, and H. Yamaguchi, "Phonon-cavity electromechanics," *Nature Physics*, vol. 8, no. 5, pp. 387–392, 2012.

[47] L. Mandel and E. Wolf, *Optical coherence and quantum optics*. Cambridge university press, 1995.

[48] D. I. Schuster, *Circuit Quantum Electrodynamics*. PhD thesis, Yale university, May 2007. Chapter 3.

[49] A. Xuereb and M. Paternostro, "Selectable linear or quadratic coupling in an optomechanical system," *Physical Review A*, vol. 87, p. 023830, Feb 2013.

[50] J. Thompson, B. Zwickl, A. Jayich, F. Marquardt, S. Girvin, and J. Harris, "Strong dispersive coupling of a high-finesse cavity to a micromechanical membrane," *Nature*, vol. 452, no. 7183, pp. 72–75, 2008.

[51] H. Hida, M. Shikida, K. Fukuzawa, S. Murakami, K. Sato, K. Asaumi, Y. Iriye, and K. Sato, "Fabrication of a quartz tuning-fork probe with a sharp tip for afm systems," *Sensors and Actuators A: Physical*, vol. 148, no. 1, pp. 311–318, 2008.

[52] R. Rasuli, M. Ahadian, *et al.*, "Mechanical properties of graphene cantilever from atomic force microscopy and density functional theory," *Nanotechnology*, vol. 21, no. 18, p. 185503, 2010.

[53] J. Bunch, T. Rhodin, and P. McEuen, "Noncontact-afm imaging of molecular surfaces using single-wall carbon nanotube technology," *Nanotechnology*, vol. 15, no. 2, p. S76, 2004.

[54] M. S. Hanay, S. I. Kelber, C. D. O'Connell, P. Mulvaney, J. E. Sader, and M. L. Roukes, "Inertial imaging with nanomechanical systems," *Nature Nanotechnology*, 2015.

[55] S. Forstner, S. Prams, J. Knittel, E. van Ooijen, J. Swaim, G. Harris, A. Szorkovszky, W. Bowen, and H. Rubinsztein-Dunlop, "Cavity optomechanical magnetometer," *Physical Review Letters*, vol. 108, no. 12, p. 120801, 2012.

[56] A. G. Krause, M. Winger, T. D. Blasius, Q. Lin, and O. Painter, "A high-resolution microchip optomechanical accelerometer," *Nature Photonics*, vol. 6, no. 11, pp. 768–772, 2012.

[57] P. Häkkinen, A. Isacsson, A. Savin, J. Sulkko, and P. Hakonen, "Charge sensitivity enhancement via mechanical oscillation in suspended carbon nanotube devices," *Nano Letters*, vol. 15, no. 3, pp. 1667–1672, 2015.

[58] J.-M. Pirkkalainen, S. Cho, J. Li, G. Paraoanu, P. Hakonen, and M. Sillanpää, "Hybrid circuit cavity quantum electrodynamics with a micromechanical resonator," *Nature*, vol. 494, no. 7436, pp. 211–215, 2013.

[59] K. C. Schwab and M. L. Roukes, "Putting mechanics into quantum mechanics," *Physics Today*, vol. 58, no. 7, pp. 36–42, 2005.

Aalto-DD 145/2015

ISBN 978-952-60-6401-7 (printed)
ISBN 978-952-60-6402-4 (pdf)
ISSN-L 1799-4934
ISSN 1799-4934 (printed)
ISSN 1799-4942 (pdf)

Aalto University
School of Science
Department of Applied Physics, Low Temperature Laboratory
www.aalto.fi

BUSINESS + ECONOMY

ART + DESIGN + ARCHITECTURE

SCIENCE + TECHNOLOGY

CROSSOVER

DOCTORAL DISSERTATIONS